OULU 2023
C 876

ACTA UNIVERSITATIS OULUENSIS

Ahmed Abdelrahim

TOWARDS LOWER CO_2 EMISSIONS IN IRON AND STEELMAKING – HYDROGEN-ASSISTED REDUCTION AND CEMENT-FREE BRIQUETTES

UNIVERSITY OF OULU GRADUATE SCHOOL;
UNIVERSITY OF OULU,
FACULTY OF TECHNOLOGY

ACTA UNIVERSITATIS OULUENSIS
C Technica 876

AHMED ABDELRAHIM

TOWARDS LOWER CO_2 EMISSIONS IN IRON AND STEELMAKING – HYDROGEN-ASSISTED REDUCTION AND CEMENT-FREE BRIQUETTES

Academic dissertation to be presented, with the assent of the Doctoral Programme Committee of Technology and Natural Sciences of the University of Oulu, for public defence in the Oulun Puhelin auditorium (L5), Linnanmaa, on 28 April 2023, at 12 noon

UNIVERSITY OF OULU, OULU 2023

Acta Univ. Oul. C 876, 2023

Supervised by
Professor Timo Fabritius
Doctor Matti Aula

Reviewed by
Professor Ko-ichiro Ohno
Professor Caisa Samuelsson

Opponent
Professor Henrik Saxén

ISBN 978-952-62-3652-0 (Paperback)
ISBN 978-952-62-3653-7 (PDF)

ISSN 0355-3213 (Printed)
ISSN 1796-2226 (Online)

Cover Design
Raimo Ahonen

PUNAMUSTA
TAMPERE 2023

Abdelrahim, Ahmed, Towards lower CO_2 emissions in iron and steelmaking – Hydrogen-assisted reduction and cement-free briquettes.
University of Oulu Graduate School; University of Oulu, Faculty of Technology
Acta Univ. Oul. C 876, 2023
University of Oulu, P.O. Box 8000, FI-90014 University of Oulu, Finland

Abstract

The European Union has set an ambitious target to limit the global temperature increase to less than 2°C. To fulfill this goal, the carbon emissions level should be reduced to 80–95% of the 1990 level by 2050. One of the most energy-intensive industries worldwide is the iron and steel industry. One approach to tackling this issue is to eliminate fossil-based reducing agents and utilize hydrogen to produce iron. Moreover, massive quantities of carbon and iron-bearing residues are generated at different stages of the steelmaking processes. In this research, the influence of hydrogen and water vapor on the reduction of acid iron ore pellets was studied in conditions simulating an operating blast furnace. Pellets reduced in a hydrogen-containing gas were found to achieve a higher reduction rate and extent, and also resulting in higher surface area and porosity. Additionally, several side streams from iron and steelmaking were used to produce cold bonded briquettes for use in a blast furnace utilizing an ettringite ($C_3A \bullet 3C\overline{S} \bullet 32H$)-based binder. The ettringite-based binder was produced primarily using ladle slag and used as an alternative to ordinary Portland cement as a binder in briquettes. Briquettes produced using ettringite-based binder were found to possess several technical, environmental, and economic advantages, including excellent compression and drop damage resistance compared to reference briquettes made using ordinary Portland cement, especially after 2 and 7 days of curing. Moreover, laboratory tests were conducted to assess the suitability of self-reducing and slag-forming briquettes produced from side streams to be used in an electric arc furnace. Briquettes were made using organic and inorganic binders. Tests were carried out to assess the mechanical, chemical, and thermal properties through a series of tests, including a thermogravimetric analyzer (TGA) coupled with a mass spectrometer (MS), dilatometry, and melting trials. Based on the laboratory test results, two briquettes out of the seven tested briquettes were deemed suitable for an electric arc furnace, three of the briquettes were considered unsuitable, and two of the briquettes were considered of limited use.

Keywords: blast furnace, cold-bonded briquettes, electric arc furnace, ettringite-based binder, hydrogen, ironmaking, melting, reduction, swelling

Abdelrahim, Ahmed, Kohti pienempiä CO_2-päästöjä raudan ja teräksen valmistuksessa – Vetyavusteinen pelkistys ja sementittömät briketit.
Oulun yliopiston tutkijakoulu; Oulun yliopisto, Teknillinen tiedekunta
Acta Univ. Oul. C 876, 2023
Oulun yliopisto, PL 8000, 90014 Oulun yliopisto

Tiivistelmä

Euroopan Unioni on asettanut kunnianhimoisen tavoitteen rajoittaa maapallon lämpötilan nousu alle 2 °C:seen. Jotta tavoitteeseen päästäisiin, vuoteen 2050 mennessä hiilidioksidipäästöjä tulisi vähentää 80–95 % verrattuna vuoden 1990 tasoon. Yksi maailman energiaintensiivisimmistä teollisuuden aloista on raudan ja teräksen valmistus. Eräs keino on vähentää fossiiliperäisten pelkistysaineiden käyttöä ja hyödyntää vetyä raudan valmistuksessa. Lisäksi valtavat määrät hiiltä ja rautaa sisältäviä sivuvirtoja muodostuu eri vaiheissa teräksen valmistuksen prosessiketjua. Tässä työssä on tutkittu vedyn ja vesihöyryn vaikutusta happamien rautapellettien pelkistymiseen masuunia jäljittelevissä olosuhteissa. Vetyä sisältävässä kaasuatmosfäärissä pelkistetyt pelletit pelkistyivät nopeammin ja saavuttivat korkeamman pelkistysasteen suuremman BET pinta-alan ja huokoisuuden ansiosta. Lisäksi useita raudan ja teräksen valmistuksen sivuvirtoja käytettiin kylmäpuristettujen masuunibrikettien valmistuksessa hyödyntäen ettringiitti ($C_3A \cdot 3C\overline{S} \cdot 32H$) -pohjaista sideainetta. Ettringiitti-pohjainen sideaine valmistettiin etupäässä senkkakuonasta ja sillä korvattiin perinteinen Portland-sementti briketin sideaineena. Ettringiitti-pohjaisesta sideaineesta valmistetuissa briketeissä havaittiin useita teknisiä, taloudellisia ja ympäristöön liittyviä etuja verrattuna Portland-sementistä valmistettuihin referenssibriketteihin kuten erinomainen puristuslujuus ja vähäinen vaurioalttius pudotuksessa erityisesti 2 ja 7 päivän kovettumisen jälkeen. Lisäksi selvitettiin sivutuotevirroista valmistettujen itsepelkistyvien ja kuonaa muodostavien brikettien soveltuvuutta valokaariuuniprosessiin laboratoriokokein. Briketeissä käytettiin sekä orgaanisia että epäorgaanisia sideaineita. Mekaanisia, kemiallisia ja korkealämpötilaominaisuuksia arvioitiin tekemällä erilaisia testejä kuten termogravimetria (TGA) yhdistettynä massaspektrometriin (MS) sekä dilatometri- ja sulamiskokeita. Laboratoriotestitulosten pohjalta seitsemästä brikettilaadusta kahden todettiin soveltuvan valokaariuuniin, kolme brikettilaatua osoittautui ei-soveltuviksi valokaariuuniin ja kahden arvioitiin soveltuvan rajoitetusti valokaariuuniin.

Asiasanat: ettringiitti-pohjainen sideaine, kylmäpuristetut briketit, masuuni, pelkistyminen, raudan valmistus, sulaminen, turpoaminen, valokaariuuni, vety

Lorem ipsum dolor sit amet

Acknowledgments

In the Name of Allah, the Most Gracious, and the Most Merciful, I praise and thank Allah for His blessings bestowed upon me, not only during my research journey but the entirety of my life.

The research work for this thesis was done in the Process Metallurgy Research Unit of the University of Oulu, Finland between 2018 and 2022. The research was part of the Online Blast Furnace Stack Status Monitoring (StackMonitor) project and Cement-free Brick Production Technology for the Use of Primary and Secondary Raw Material Fines in EAF Steelmaking (Fines2EAF) project, both financed by the Research Fund for Coal and Steel (RFCS) of the European Community and by the TOCANEM project. Support from SSAB Europe Oy (Finland) is highly appreciated for providing the materials used in this research work.

I am most thankful to my principal supervisor, Professor Timo Fabritius, for allowing me to work at the Process Metallurgy Research unit, for allowing me such a degree of freedom during my research, for the endless support and understanding, and for the countless hours of discussions and meetings. I am forever grateful.

I also express my gratitude to my second supervisor, Matti Aula, PhD., for his valuable guidance and suggestions, for pushing me forward, and for taking so much time and effort to help me with my publications. I have learned so much from him. Special thanks go to Doctor Mikko Iljana for assisting me with experimental work and engaging in valuable discussions.

I sincerely thank the official pre-examiners of this thesis, Professor Ko-ichiro OHNO and Professor Caisa Samuelsson, for their invaluable evaluation of the thesis manuscript and their thoughtful comments and suggestions to improve the thesis quality.

I am thankful to Professor Eva Pongrácz, PhD., the chairman of my thesis follow-up group. I am grateful to have been one of her students after arriving in Finland. Not only is she a great professor but she is a very kind and compassionate person. I thank her for everything. I would also like to thank Aleksi Laukka, PhD., for being part of my thesis follow-up group and for his valuable feedback and constructive discussions.

I extend a special thanks to the Egyptian and Arab community members, staff, and alumni at the University of Oulu: Abdulrahman, Ahmed Albiltagy, Amr Hamada, Dr. Atef, Ayman Hamdallah, Eslam Eldeeb, Hassaan Elsayed, Islam Ibrahim, Dr. Khaled Abbas, Khaled Elkhouly, Mahmoud Mohamed, Mohamed Zaghloul,

Mohamed Salah, Mostafa Ismail, Omar Elshinnawy, Sherif Elashmawy, and many others. They were more than friends and colleagues; they were family. Because of them, I never felt alone, and Oulu has felt like my home since day one. I would also like to thank my life-long friends, Ahmed Abdelfatah, Ahmed Senshe, Ahmed Srag, Ahmed Yehia, Hatem Ahmed, Nada, Moataz Mahmoud, Mohamed Saeed, and Mostafa Mohamed, as well as many others who never stopped being my best friends regardless of the distance and years apart.

I would like to acknowledge the Tauno Tönning foundation, the Finnish Cultural Foundation, Steel and Metal Producers' Fund, and the Walter Ahlström foundation for their financial support.

I would also like to acknowledge Mr. Tommi Kokkonen and Mr. Riku Mattila from the Process Metallurgy research unit at the University of Oulu for their technical support and everything they taught me, for the fruitful discussions, and for always being there, trying their best to help.

I am also grateful for my future wife, whom I do not yet know and have not yet met. Thank you for being slightly late and giving me much-needed time to complete my doctoral studies.

My warmest thanks belong to my family, especially my mother, Fatima, my dad, Abdelmonem, my sisters, Dalia and Yasmine, and my brother, Mohamed. I thank them for everything they have done for me: for their love, care, and support. I cannot start to express how much I love all of them. Being so far apart has been challenging and would have been unbearable if it were not for their support.

Finally, I would like to thank my parents, once again and million times over, because thanking them once is never enough. I love you!

Oulu, April 2023 Ahmed Abdelrahim

List of abbreviations and symbols

AIRI	Adjusted impact resistance index
BET	Brunauer, Emmett, and Teller method
BF	Blast furnace
BFS	Blast furnace simulator
C-S-H	Calcium silicate hydrate
DTG	Derivative thermogravimetry
EAF	Electric arc furnace
EDS	Energy-dispersive X-ray spectrometer
e.g.	Exempli gratia
FA	Ferroalloy
FESEM	Field emission scanning electron microscope
G	Gypsum
GGBFS	Ground granulated blast furnace slag
IA	Image analysis
i.e.	Id est
IEA	International energy agency
IRI	Impact resistance index
LS	Ladle slag
LSG	Ettringite-based binder from ladle slag and gypsum
LSCM	Laser scanning confocal microscope
NPT	Normal pressure and temperature
MPVP	Multi-point vertical probing
MS	Mass spectrometry
OPC	Ordinary Portland cement
OM	Optical microscope
PSD	Particle size distribution
SEM	Scanning electron microscope
TGA	Thermogravimetric analysis
XRD	X-ray powder diffraction
XRF	X-ray fluorescence

Symbols

σ_c	Compression strength in MPa
F	Force at which the briquette suddenly fails in N

A	Cross-section area of tested briquette in mm^2
η_{CO}	CO gas utilization numerical index
η_{H_2}	H_2 gas utilization numerical index
m_1	Mass of the pellet sample prior to reduction, in grams
m_2	Mass of the sample after reduction, in grams
w_1	Iron (II) oxide mass percentage in a sample before reduction
w_2	Total iron mass percentage in the sample before reduction
R	Reduction degree
ρ_s	Skeletal density
ρ_e	Envelope density
ε	Pellet porosity

In this thesis, standard cement chemistry notations were used as follows:

A	Al_2O_3
C	CaO
S	SiO_2
$\bar{S}$	SO_3

List of original publications

This thesis is based on the following publications, which are referred to throughout the text by their Roman numerals:

I. Abdelrahim, A., Iljana, M., Omran, M., Vuolio, T., Bartusch, H., & Fabritius, T. (2020). Influence of H_2–H_2O content on the reduction of acid iron ore pellets in a CO–CO_2–N_2 reducing atmosphere. *ISIJ International*, *60*, 2206. https://doi.org/10.2355/isijinternational.ISIJINT-2019–734

II. Abdelrahim, A., Nguyen, H., Omran, M., Kinnunen, P., Iljana, M., Illikainen, M., & Fabritius, T. (2022). Development of cold-bonded briquettes using by-product-based ettringite binder from ladle slag. *Journal of Sustainable Metallurgy*, *8*(1), 468–487. https://doi.org/10.1007/s40831–022–00511–1

III. Abdelrahim, A., Aula, M., Iljana, M., Willms, T., Echterhof, T., Steinlechner, S., Mombelli, D., Mapelli, C., Omran, M., Preiss, S., & Fabritius, T. (2021). Suitability of self-reducing and slag-forming briquettes for electric arc furnace use based on laboratory tests. *Steel Research International*, 2100472. https://doi.org/10.1002/srin.202100472

The author of this thesis was the primary author of all three publications. The author's contribution to the publications was as follows: major planning of the publications' content, reviewing the relevant literature, conducting the majority of experimental work, analyzing experimental results, drawing conclusions, and writing.

In addition to the articles upon which this thesis was based, the following publications also belong to the author. Although they are outside the direct scope of this thesis, these publications provided background information that was complementary to the original publications used in this thesis:

IV. Echterhof, T., Willms, T., Preiss, S., Aula, M., Abdelrahim, A., Fabritius, T., Mombelli, D., Mapelli, C., Steinlechner, S., & Unamuno, I. (2019). Fabrication of agglomerates from secondary raw materials reinforced with paper fibres by stamp pressing process. *Applied Sciences*, *9*(19), 3946. https://doi.org/10.3390/app9193946

V. Iljana, M., Abdelrahim, A., Bartusch, H., & Fabritius, T. (2022). Reduction of acid iron ore pellets under simulated wall and center conditions in a blast furnace shaft. *Minerals*, *12*(6), 741. https://doi.org/10.3390/min12060741

VI. Khalifa, A., Bazhin, V., Kuskova, Y., Abdelrahim, A., & Ahmed, Y. (2021). Study the recycling of red mud in iron ore sintering process. *Journal of Ecological Engineering*, *22*(6), 191–201. https://doi.org/10.12911/22998993/137966

VII. Omran, M., Fabritius, T., & Abdelrahim, A. (2020). Effect of metallurgical waste properties on determining suitable recycling method. *Key Engineering Materials*, *835*, 297–305. https://doi.org/10.4028/www.scientific.net/KEM.835.297

VIII. Willms, T., Echterhof, T., Steinlechner, S., Aula, M., Abdelrahim, A., Fabritius, T., Mombelli, D., Mapelli, C., & Preiss, S. (2020). Investigation on the chemical and thermal behavior of recycling agglomerates from EAF by-products. *Applied Sciences*, *10*(22), 8309. https://doi.org/10.3390/app10228309

Contents

1 Introduction

1.1 Background

The European Union has set an ambitious target to limit the global temperature increase to less than 2 °C. To fulfill this goal, the carbon emissions level should be reduced to 80–95% of the 1990 level by 2050. One of the most energy-intensive industries worldwide is iron and steel industry. The electric arc furnace (EAF) and blast furnace (BF) routes are the most commonly used routes to produce steel. The former conventionally uses electric energy to melt scrap. The latter utilizes coke as a reducing agent and conventionally utilizes sinter, pellets, and lump ore as the iron-bearing feed material. In 2020, 73.2% of steel was produced through the BF route while 26.3% was produced through the EAF route (Worldsteel association, 2022). The steel industry accounts for around 4–5% of the total man-made greenhouse gases in the world (Cavaliere, 2016). According to the International Energy Agency (IEA), the iron and steel industry accounts for the largest share of CO_2 emissions from the global manufacturing sector at about 27% (Ministry of Economic Affairs and Employment et al., 2019). Each ton of steel produced through the BF route results in 1.9–2.1 tons of CO_2 (Cavaliere, 2016; Raabe et al., 2019).

Finland has set a goal to become a global leader in circular economies by 2025, to achieve carbon neutrality by 2035, and to become "the first fossil-free welfare society" by 2035 (Ministry of Economic Affairs and Employment et al., 2019). Efforts made toward these goals include the shutdown of sintering plants, which are emissions-intensive sources. Moreover, researchers have focused on the minimization of fossil-based reducing agents and on utilizing more hydrogen in the production of iron (Kemppainen et al., 2012). Minimizing fossil-based reducing agents and transitioning to hydrogen-rich reduction requires a deeper and better understanding of processes and reactions within BF and its different zones, as well as a better understanding of the iron burden's behavior and properties as it descends the BF. Under the increasingly strict global environmental standards, the hydrogen reduction route of iron production is becoming more and more attractive.

Massive quantities of carbon and iron- bearing wastes are generated at different stages of the iron- and steelmaking processes. The waste includes fines, dust, sludge, and mill scale (Omran et al., 2020). Side streams generated during EAF steel production are estimated to be around 181.4 kg per ton of crude steel produced (Ndlovu et al., 2017). The EAF steelmaking route is associated with lower capital

costs and higher process flexibility. Steel production through the EAF route is expected to increase due to the transition to hydrogen-based reduction. Therefore, the total volume of side streams, such as dust, sludge, and slags from EAF steelmaking, is expected to increase as a result (Ndlovu et al., 2017; Suetens et al., 2014). Several methods have been innovated to allow better utilization of side streams from iron and steelmaking. Such methods include agglomeration techniques, such as pelletizing and briquetting. Briquettes are agglomerates that are usually made of a mixture of fine iron and fine carbonaceous materials before adding some organic or inorganic binding agents, such as ordinary Portland cement (OPC). One downside to the use of cement in briquette-making is cement production–related CO_2 emissions. The cement industry contributes more than 5% of the total anthropogenic carbon dioxide emissions in the world (Mahasenan et al., 2003).

Several researchers have studied the use of briquettes in the EAF process in order to recycle metal oxides and create slag foaming (Bagatini et al., 2017; Davydenko et al., 2015, 2019; Yang et al., 2009). Iron-bearing materials used as feed for BFs are conventionally tested for their chemical properties, mechanical strength, reducibility, softening and melting properties, and reducibility (Geerdes et al., 2015). However, the utilization of briquettes in EAF is not highly standardized at the present.

1.2 Aim and scope

This thesis aims to minimize emissions and increase recycling within iron- and steelmaking. To achieve this target, two pathways will be the focus of this thesis. First, the influence of hydrogen on the reduction behavior of acid iron ore pellets will be studied in simulated BF conditions. This will provide insights regarding how microstructure, minerology, reduction extent, and reduction rate are affected by H_2-H_2O content in a CO-CO_2-N_2 gas. Second, the research focuses on developing a more sustainable recycling approach by producing agglomerates utilizing environmentally friendly binders rather than Portland cement and on testing the suitability of different types of briquettes to be used in EAFs through laboratory tests.

The objectives of the research are parallel to those set by Finnish government strategy on “Bio-economy and Clean Solutions,” which aims to ensure the breakthrough of a circular economy. The research involved 1) reduction and swelling laboratory scale tests of acid iron ore pellets in reducing atmosphere

containing hydrogen and water vapor and 2) briquette production and testing using several organic and inorganic binders as substitutes for cement. An ettringite-based binder utilizing ladle slag and gypsum (LSG) was studied. The binder performance was assessed as an alternative to the conventional Portland cement binder currently used in briquette making. Starch and sodium silicate were also used in the study as binders in the making of self-reducing and slag-forming briquettes.

This research addresses the following research questions:

1. How are acid iron ore pellets' microstructure and minerology influenced by varying temperature and reducing atmosphere (H_2-H_2O-CO-CO_2), simulating the conditions of a BF?
2. In terms of mechanical and chemical properties, how suitable is ettringite binder from ladle slag for use as a cement substitute in cold bonded briquettes?
3. How can the suitability of self-reducing and slag-forming briquettes for EAF use be assessed based on laboratory tests?

Fig. 1 shows the different stages of work carried out in this thesis with boundaries indicating the scope of each of the publications.

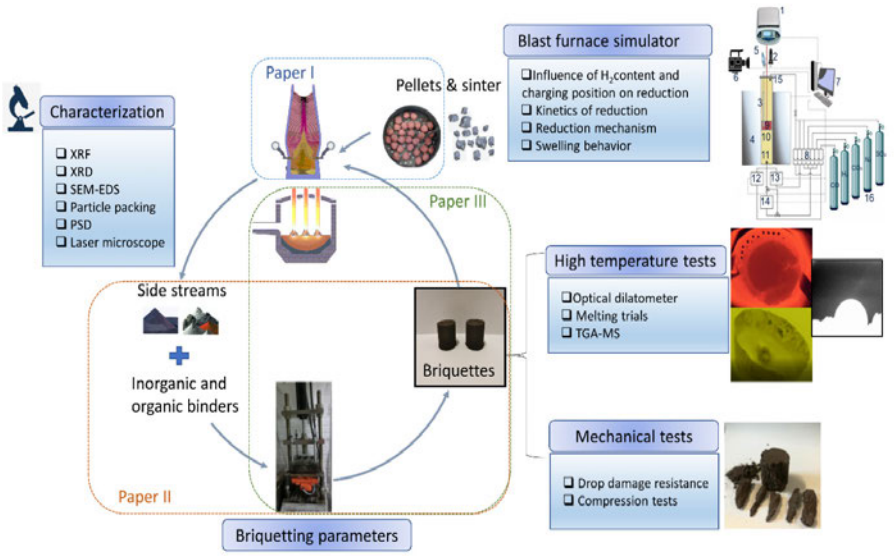

Fig. 1. Schematic showing different stages of work.

2 Fundamentals

2.1 Carbon and hydrogen-based reduction in a blast furnace

2.1.1 Blast furnace process

Environmental regulations have grown more and more strict in recent years, which has resulted in a need to transform carbon intensive industries to more environmentally conscious ones. The iron- and steelmaking industry is one of the main industries responsible for CO_2 emissions. In a BF, 400–500 kg of carbon are used in producing a ton of cast iron (Cavaliere, 2016). The carbon is used in the process of reducing iron oxides to metallic iron.

The BF is the dominant route in the ironmaking industry. A BF is a tall vertical shaft furnace that utilizes refractory bricks a as furnace lining. The charge of the BF consists primarily of iron ore, coke, and limestone. The charge is introduced at the top of the furnace in alternating layers. Pre-heated air is compressed and introduced into the furnace through tuyeres at a temperature of 1000–1300 °C. Carbon-based materials are gasified by the hot air at a temperature in the range of 1900–2300ºC. Ascending gases consisting primarily of CO, N_2, and CO_2 heat up the coke, which results in the melting of the iron ore. Slag and hot metal are produced through the melting of the iron burden, and the iron burden's oxygen is removed through chemical reactions (Geerdes et al., 2015; Ghosh & Chatterjee, 2010).

The reactions between carbon and oxygen are shown in Equations. (1) and (2):

$$\mathrm{C(s) + O_2(g) = CO_2(g)} \tag{1}$$

$$\Delta H^0 = -393.7 \times 10^3\ \mathrm{J \cdot mol^{-1}} \text{ at } 298\ \mathrm{K}$$
$$\mathrm{C(s) + \frac{1}{2}O_2(g) = CO(g)} \tag{2}$$
$$\Delta H^0 = -110.6 \times 10^3\ \mathrm{J \cdot mol^{-1}} \text{ at } 298\ \mathrm{K}$$

2.1.2 Boudouard reaction

At the tuyere level, oxygen is converted into CO and CO_2. The product of this reaction is essentially CO and not CO_2, as CO_2 is not stable above approximately 1000 °C in the presence of carbon (Biswas, 1981). Therefore, at the bosh and stack, reaction (3) must be considered:

$$CO_2(g) + C(s) = 2CO(g). \quad (3)$$

Reaction (3) is the combination of reactions (1) and (2). Reaction (3) is called the Boudouard reaction but is generally referred to as the gasification reaction. In a BF, the forward reaction is referred to as the solution loss reaction (Ghosh & Chatterjee, 2010).

2.1.3 Iron–oxygen system equilibrium

Iron oxide reduction thermodynamics has been the focus of several books (Biswas, 1981; Ghosh & Chatterjee, 2010; Seetharaman, 2005; Turkdogan, 2010). Iron forms in the ores of oxides that have three stable phases: hematite (Fe_2O_3), magnetite (Fe_3O_4), and wüstite (Fe_xO), an oxygen-deficient non-stoichiometric compound. The fields of existence of the iron oxides have been studied, and a Fe-O phase diagram is shown in Fig. 2 (Darken & Gurry, 1946).

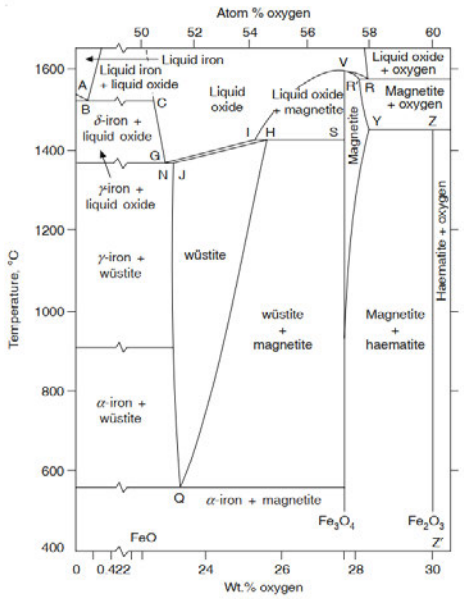

Fig. 2. Iron–oxygen phase diagram (Ghosh & Chatterjee, 2010) based on iron–oxygen phase diagram (Darken & Gurry, 1946).

2.1.4 Reduction of iron oxides by CO

In a BF, hematite is reduced to metallic iron in stepwise reactions, as in the following:

$$\text{Hematite } (Fe_2O_3) \rightarrow \text{ magnetite } (Fe_3O_4) \rightarrow \text{ wustite } (Fe_xO) \rightarrow \text{ metallic iron (Fe)}$$

As CO_2 is unstable above 1000 °C in the presence of carbon, the burning of coke at the tuyeres level generates CO, which reduces the iron burden. Below 1000 °C, reduction takes place, and CO_2 is generated as a product (Biswas, 1981).

$$3Fe_2O_3(s) + CO(g) = 2Fe_3O_4\ (s) + CO_2(g) \qquad (4)$$

$$\Delta H^0 = -52.8 \times 10^3\ J \cdot mol^{-1}$$

$$Fe_3O_4\ (s) + CO(g) = 3FeO\ (s) + CO_2(g) \qquad (5)$$

$$\Delta H^0 = +36.3 \times 10^3 \, J \cdot mol^{-1}$$
$$FeO\,(s) + CO(g) = Fe\,(s) + CO_2(g) \quad (6)$$

$$\Delta H^0 = -17.3 \times 10^3 \, J \cdot mol^{-1}$$

Below 570 °C, magnetite is reduced to metallic iron, according to the following reaction:

$$Fe_3O_4(s) + 4CO(g) = 3Fe(s) + 4CO_2(g) \quad (7)$$

The reduction of magnetite by CO and H_2 constitutes indirect reduction, while reduction by carbon is direct reduction. However, in direct reduction, the reaction takes place indirectly through a gas phase above 1000 °C; the overall reaction consumes carbon, with one step being the gasification reaction in (3) and indirect wüstite reduction in (6). The sum of reactions (3) and (6) yields the following:

$$FeO(s) + C(s) = Fe(s) + CO(g) \quad (8)$$

$$\Delta H^0 = +140.1 \times 10^3 \, J \cdot mol^{-1}$$

2.1.5 Reduction of iron oxides by H_2

The injection of steam, pulverized coal, and hydrocarbons such as oil or natural gas at the tuyere level has been traditionally practiced. Such a practice results in the formation of volatile compounds, which in turn become a source of hydrogen (Ghosh & Chatterjee, 2010). Steam also reacts with coke at high temperatures, resulting in the formation of hydrogen, according to the following reaction:

$$H_2O(g) + C\,(s) = CO(g) + H_2(g) \quad (9)$$

$$\Delta H^0 = +131.4 \times 10^3 \, J \cdot mol^{-1}$$

At the tuyere level, where the temperature is around 1900 °C, water is converted into hydrogen. Therefore, a water–gas reaction must be considered:

$$H_2(g) + CO_2(g) = H_2O(g) + CO(g) \quad (10)$$

$$\Delta H^0 = 32.0 \times 10^3 \text{ J} \cdot \text{mol}^{-1} \text{ at } 298 \text{ K}$$

Similar to CO, H_2 is a reducing agent. The reduction equation of iron oxides by hydrogen could be expressed as follows:

$$3Fe_2O_3(s) + H_2(g) = 2Fe_3O_4(s) + H_2O(g), \quad (11)$$

$$Fe_3O_4(s) + H_2(g) = 3FeO(s) + H_2O(g), \quad (12)$$

$$FeO(s) + H_2(g) = Fe(s) + H_2O(g). \quad (13)$$

The equilibrium of CO/CO_2 and H_2/H_2O for iron oxide reduction at varying temperatures is shown in Fig. 3.

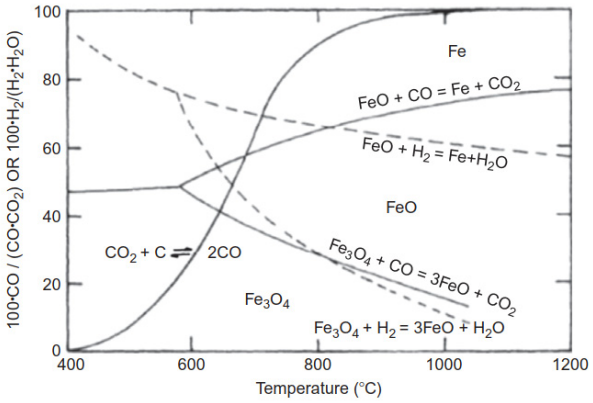

Fig. 3. Equilibrium diagram of iron oxide reduction with CO and H_2 with imposed Boudouard reaction (Seetharaman et al., 2014).

Although studied for decades, the reduction of iron oxides by hydrogen is not yet fully understood (S.-H. Kim et al., 2021). One of the challenges preventing the use of hydrogen in the iron and steel industry is the unavailability of hydrogen in quantities that would be sufficient for the industry's demands due to technical and

economic reasons (Hasanbeigi et al., 2014). Moreover, due to the endothermic nature of hydrogen reduction, an increase beyond certain limit would require the use of more coke to provide energy (Yilmaz et al., 2017).

Various reactor types are typically used to study the reduction of iron oxides, including thermogravimetric analyzers (TGAs), packed bed reactors, and fluidized bed reactors (Oh & Noh, 2017). Several researchers have studied the influence of hydrogen content on the reduction of iron oxides at different temperatures (Kemppainen et al., 2012; S.-H. Kim et al., 2021; Pineau et al., 2006, 2007; Qie et al., 2017; Wagner et al., 2006). It was found that below 900 °C, the reduction rate increases considerably when hydrogen content is increased from 15 to 20%. On the other hand, the influence of a hydrogen increase on iron oxide reduction at a temperature of 1000 °C is greater when hydrogen content is increased from 10 to 15%, and it was concluded that hydrogen content in a gas injection to a BF should be maintained between 5 and 15% (Qie et al., 2017). While some researchers have concluded that an H_2 content of less than 5% in the gas composition has little effect on reduction (Qie et al., 2017), others have concluded that an H_2 addition of up to 5% significantly increases the degree of reduction and that a further 5% addition results in much less improvement (Kemppainen et al., 2012). At later stages of the reduction of iron oxides in CO-H_2 mixtures, it is believed that the formation of a product-dense layer results in the poor diffusion of reducing gases (Kemppainen et al., 2012; Qie et al., 2017). Some researchers believe that the formation of a dense iron layer should take place at a temperature above 850 °C when dry hydrogen is employed as the reducing gas but that the temperature of dense iron formation becomes 800 °C when a mixture of hydrogen and water vapor is employed in reduction (Wagner et al., 2006). Other researchers have reported on the formation of dense iron layer when reducing hematite above 450 °C (Pineau et al., 2006, 2007). Moreover, some believe that the classical core-shell model does not fully explain the process of reduction by hydrogen and have suggested that the outbound diffusion of oxygen plays a major role in the kinetics of reduction (S.-H. Kim et al., 2021).

2.2 The use of by-product-based ettringite binder from ladle slag

2.2.1 Ladle slag

In the European Union, 48 million tons of ferrous slag are produced annually (Handley & Basuyau, 2019). Slag types include BF slag, basic oxygen furnace slag, EAF slag, and ladle slag. The use of slags originating from iron and steelmaking industry as a cement alternative would result in a significantly reduced amount of landfilled slag. Moreover, it would contribute to the conservation of natural resources and the reduction of emissions from the cement industry.

Ladle slag, one of the side streams from the iron and steel industry, is either used in low-value applications or disposed of in landfills. Ladle slag originates from the final stages of steelmaking after liquid steel is poured into a ladle furnace, where it is subject to deoxidation and desulphurization and where alloying elements are added (Setién et al., 2009). The composition of ladle slag varies depending on the working practice of each individual steel manufacture and the nature of the heat used (Posch et al., 2002). Calcium aluminates and calcium silicates are the main mineral phases in ladle slag, which has CaO/SiO_2 ratio of around 2:1(Choi et al., 2016; Shi, 2002). Ladle slag typically contains less than 3% FeO. However, depending on the steel shop, FeO content could be as high as 10% (Koros, 2003). Compared to other types of slags, ladle slag typically contains high Al_2O_3 content. However, Al_2O_3 and ladle slag basicity could vary significantly, as some sources have reported a CaO/SiO_2 ratio of up to 8:1 and Al_2O_3 content to be as low as 1.3% (Adesanya et al., 2017; Adolfsson et al., 2011; Papayianni & Anastasiou, 2012; Rađenović et al., 2013; Shi & Hu, 2003). Ladle slag has the potential to be used in several applications, such as agriculture, construction, aquiculture, and soil stabilization (Dippenaar, 2005; Manso et al., 2005; Proctor et al., 2000).

2.2.2 Ettringite-based binder

Many researchers have pointed out the potential of ladle slag as a precursor for cementitious materials. Ettringite-based binders are potential substitutes for OPC. Ettringite is a common hydrate in Portland cement and is formed as a result of chemical reaction between solid calcium aluminate and calcium sulfate sources (Winnefeld & Lothenbach, 2010). In the presence of gypsum, it can form according to the following reaction:

$$C_3A + 3C\bar{S} + H_2 + 26H \rightarrow C_6A\bar{S}3H_{32} \quad (14)$$

OPC consists mainly of four major crystalline phases: tricalcium silicate, dicalcium silicate, tricalcium aluminate, and tetracalcium aluminoferrite. Although raw materials used in the production of OPC are available and affordable, its manufacturing is responsible for significant emissions of carbon dioxide (up to 913 kg CO_2/t) and is accompanied by high energy demands during the firing and subsequent grinding of the final clinker (De Belie et al., 2018).

Ettringite-based binders are considered to be an attractive alternative to OPC. Due to the low clinkering temperature and the use of industrial side streams in their production, they are associated with low CO_2 emissions. Moreover, ettringite-based binders are associated with other attractive properties, such as fast setting, good mechanical properties, high chloride resistance, and heavy metal immobilization (Luz et al., 2007; Peysson et al., 2005). Al-rich slag with calcium sulfate sources could be used to produce ettringite-based binders (Nguyen et al., 2019). Ladle slag has been used to produced ettringite-based binders in the presence of dehydrated gypsum ($CaSO_4$) (J.-M. Kim et al., 2016).

2.3 Assessing the suitability of self-reducing and slag-forming briquettes for EAF use based on laboratory tests

With around 26.3% of world crude steel being produced through the EAF route, several side streams are generated in high quantities. For each ton of crude steel produced through the EAF route, 1841.4 kg of side streams are produced (Ndlovu et al., 2017). EAF steel production process is highly flexible and is associated with lower capital cost. Moreover, due to the transition to hydrogen-based reduction and increased recycling, the volume of steel produced through the EAF route is expected to increase, and the amount of side streams generated are expected to increase in turn (Gordon & Kumar, 2013; Suetens et al., 2014). Although some of EAF side streams are considered hazardous (de Araújo & Schalch, 2014), the side streams contain several valuable elements (Gao et al., 2012). EAF dust, for example, contains around 30–40% zinc and 20% iron (Magdziarz et al., 2015). Side streams from EAF may undergo several beneficiation techniques, including thermal and hydrometallurgical methods to recover valuable elements (Rao, 2006). Leaching and recovering valuable methods with a Waelz kiln are some of the methods used to recover zinc. However, these methods face limitations, such as the

need for metal content to be high enough for extraction (de Araújo & Schalch, 2014). Briquetting is one of the important techniques employed to recycle side streams back into the steelmaking process (Godinskii et al., 2003). By utilizing less expensive side stream materials in the steelmaking process, production costs could be reduced, and the internal recycling would reduce the cost of disposing of side streams (Toulouevski & Zinurov, 2013).

Employing an EAF to produce steel involves the steps of handling the charge material, charging the material to the furnace, and melting and refining (Ndlovu et al., 2017). When briquettes are used as a charge material, they are subject to different forces during these steps, and their behavior should be evaluated to assess their suitability to act as a feed material in the production process.

Briquettes must possess adequate mechanical properties to withstand their handling at the scrap yard and the subsequent feeding through a silo. This is important so that briquettes do not crumble under the load. While a standard is available to assess the crushing strength of pellets used in a BF (British Standards Institution, 2015), no standard is available to assess this property for briquettes used in an EAF. However, it has been reported that industrial briquettes should be able to withstand a compression strength of at least 350 kPa, which corresponds to the maximum load they are subjected to during the filling of a load bucket (Richards, 1990). Others have suggested that briquettes should be able to withstand 100 kg/briquette (Kumar et al., 2017). Some researchers assessed briquettes' mechanical properties using the tumbler standard test (British Standards Institution, 2007a; López & López-Delgado, 2002). Although the optimum tumbler index according to the standard for sinter and pellets is considered to be 70 and 90%, respectively (Geerdes et al., 2015), researchers have considered that a tumbler index higher than 55% is adequate for briquette use.

Briquettes must also be able withstand a drop from certain height and the accompanied mechanical stress, as one of the main contributors to dust generation in an EAF is the fly-off arising from the charging procedure (Guézennec et al., 2005). Drop damage–resistance testing involves repeatedly dropping briquettes onto a steel plate and observing mass loss after the drops. Some researchers have suggested that a briquette should withstand seven to nine drops in industrial conditions, which is similar to the number of drops that lime lumps can withstand in industrial conditions (Jarnerud et al., 2019). However, the specifics of the testing methods employed by researchers significantly varied; For example, some researchers chose to test briquettes by dropping them from a height of 0.3 m (El-Hussiny & Shalabi, 2011), others from a height of 1 m (Mousa et al., 2017), others

from a height of 2 m (Demus et al., 2016; Magdziarz et al., 2015), and others from a height of 4 m (Paknahad et al., 2019). Drop damage resistance is usually expressed as the number of drops before breakage or a loss of 50% of the initial mass. Drop damage resistance can also be expressed as a percentage of fines generated after a certain number of drops. Although no standard is available to assess the drop damage resistance of briquettes, standards are available for coke and coal drop shatter testing (ASTM International, 2018, 2019). Some researchers have suggested other testing parameters that could better assess the drop damage resistance of briquettes (Blesa et al., 2003). The Parameters Impact Resistance Index (IRI) and Adjusted Impact Resistance Index (AIRI) are determined based on the number of pieces and powder generated following briquette drops.

3 Material

3.1 Iron ore pellets (related to Publication I)

In this study, acid iron ore pellets were obtained from ROGESA (Roheisengesellschaft) in Dillingen, Germany. Pellets were used in a series of isothermal reduction tests in a blast furnace simulator (BFS). The chemical composition of the used pellets is shown in Table 1. A total of 30 pellets with a size range of 10–12.5 mm were used in each isothermal test with a total weight of 100 ± 0.1 grams. Special care was taken to ensure that the pellets chosen were free of cracks and round in shape.

Table 1. Chemical composition of the acid pellets used in Publication I (wt.%) (Modified under CC BY-NC-ND 4.0 license from Publication I © 2021 The Iron and Steel Institute of Japan).

Chemical composition	Acid pellets (%)
TFe	64.59
FeO	< 0.1
SiO_2	6.0
CaO	1.2
MgO	0.73
Al_2O_3	0.39
Na_2O	0.09
K_2O	0.05

3.2 Side streams from steelmaking

3.2.1 Side streams from BF steelmaking (related to Publication II)

Nine different types of side stream material were obtained from the SSAB steelmaking plant in Raahe, Finland. Two types of briquettes were produced. The first type utilized ordinary Portland cement (OPC) and ground granulated blast furnace slag (GGBFS) cement, and it acted as a reference briquette, and the second type utilized varying amounts of ettringite-based binder with no Portland cement. The briquettes were produced at a lab scale using a vibrating briquetting machine. The parameters of the briquetting process were optimized, including moisture

content, vibration time, particle packing, briquetting force, and curing duration and conditions.

Various types of lab equipment laboratory equipment were used in this research to study the side streams characteristics.

3.2.2 Side streams from EAF steelmaking (related to Publication III)

Side streams used to produce briquettes to be recycled for use in an EAF were obtained mainly from two EAF steel plants in Europe. The side streams and their sources are shown in Table 2.

Table 2. Origin of side streams used to produce EAF briquettes (Adapted, with permission, from Publication III © 2021 Wiley-VCH GmbH).

Side stream	Origin
Ladle furnace slag_1	Collected from plant No.1 secondary metallurgy ladle furnaces.
Ladle furnace slag_2	Collected from plant No.2 secondary metallurgy ladle furnaces.
Mixed residues	Collected in plant No.2 and consist of mixture of different remaining materials generated in the steel plant (from metallurgical hall to the rolling mill).
Belt conveyor fines	Collected in plant No.3 and consist of mixture of different materials added through the belt conveyor in the EAF and are rich in CaO.
Oxy-cutting fines	Collected in plant No.3 from the off gases from the cutting of billets in the continuous casting area.
Combustion chamber dust	Collected in plant No.3 in a box in the combustion chamber at the off-gas duct, where the remaining combustible components of the off-gases are post combusted.
Grinding sludge	Collected from a bearing manufacturer near plant No.3.
Ferromanganese carbon dust	Consists of filtering system dusts obtained from the duct at FeMnC production site.

3.2.3 Physical properties of side streams

The physical and chemical properties of the received side streams were assessed. A conning and quartering method was used to obtain a representative sample of each side stream (British Standards Institution, 1986). To obtain dry samples and determine their moisture content, samples were left in a lab oven overnight at 105 °C. Side stream samples' apparent densities were determined according to ISO standards (British Standards Institution, 1998), using equation (15):

$$\text{Bulk density} = \frac{\text{Sample mass}}{\text{Volume of the sample}} \quad (15)$$

To determine the skeletal densities (ρ_S) of the side streams, a gas pycnometer, AccuPyc II 1340, was used. The gas pycnometer employed helium as the displacement gas, and the sample chamber capacity was 10 cm^3. While true density is defined based on the material volume excluding open and closed pores, skeletal density excludes only the open pores. Skeletal density was determined based on the average of three measurements taken by the gas pycnometer. Table 3 shows the bulk and skeletal densities, moisture content, and voidages of side streams used to produced reference and LSG briquettes. A similar approach was employed to determine the moisture content and densities of side streams used to produce briquettes to be used in EAFs. The moisture content and bulk and skeletal densities of EAF side streams are shown in Table 4.

Table 3. Bulk and skeletal densities, moisture content and voidages of side streams used to produced ettringite-based binder briquettes.

#	Raw material	Moisture content (db %)	Bulk density (kg/m^3)	Skeletal density (kg/m^3)	Voidages (%)
1	Coarse pellet fines	1.89	2579.10	4974.40	48.15
2	Fine pellet fines	3.15	2688.50	4957.40	45.77
3	BF stock/cast house dust	23.59	1089.93	2717.60	59.89
4	Coke dust	0.06	364.75	1993.50	81.70
5	Premix (60:40 steel scrap and BF top dust)	6.98	2076.14	4216.50	50.76
6	Briquette fines	8.03	1725.73	3471.00	50.28
7	Desulfurization scrap	15.01	1519.49	3878.30	60.82
8	Mill scale	4.43	2676.13	5440.40	50.81
9	Steel scrap	5.42	2406.33	4740.50	49.24

Table 4. Bulk and skeletal densities, moisture content, and voidages of side streams used to produced EAF briquettes (Adapted, with permission, from Publication III © 2021 Wiley-VCH GmbH).

Material	Moisture content (%)	Bulk density (g/cm^3)	True density (g/cm^3)
Ladle furnace slag 1	0.18	1.32	3.24
Ladle furnace slag 2	0.00	1.24	3.33
Mixed residues	13.56	1.51	2.93
Belt conveyer fines	-	1.03	3.66
Oxy cutting fines	4.73	1.82	4.74

Material	Moisture content (%)	Bulk density (g/cm^3)	True density (g/cm^3)
Combustion chamber dust	6.40	2.19	4.28
Grinding sludge	24.79	1.19	5.30
Ferromanganese carbon dust	3.98	0.75	3.23

The particle size distribution (PSD) of side streams from BF steelmaking was determined in two steps. In the first step, a commercially available Analysette 3 Pro Vibratory Sieve Shaker from Fritsch, Germany, was used to obtain the PSD of a coarser fraction of each sample (>2 mm) and to separate the finer fraction (<2 mm) of the sample particles. In a subsequent step, a Beckman Coulter LS 13 320 Universal Liquid Module Laser Diffraction Particle Size Analyzer was used to obtain PSD of the finer fraction (<2 mm). The complete PSD of the used side streams is shown in Fig. 4.

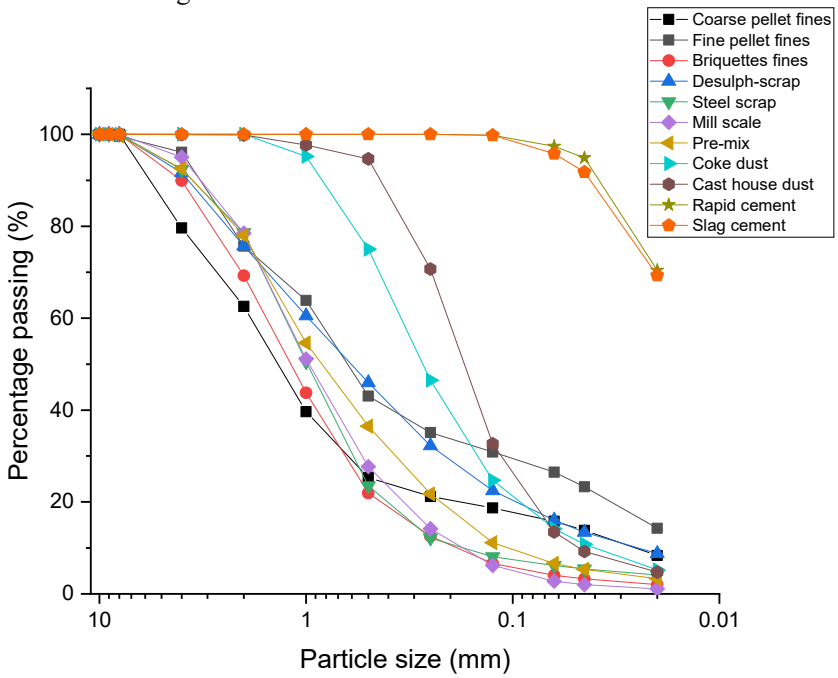

Fig. 4. Particle size distribution of side stream material used to produce reference and LSG briquettes (Reprinted under CC BY 4.0 license from Publication II © 2022 Authors).

3.2.4 Chemical properties and minerology of side streams

The chemical composition of side streams was determined using X-ray fluorescence (XRF) analyses. A calibrated Panalytical Axios Max wavelength-dispersive spectrometer equipped with a rhodium anode tube was employed for the XRF analysis. Table 5 and Table 6 show the chemical composition of the side streams used to produce ettringite-based binder briquettes.

Table 5. Chemical composition of side streams used to produce ettringite-based binder briquettes (Reprinted under CC BY 4.0 license from Publication II © 2022 Authors).

Element	Fine pellet fines	Coarse pellet fines	Cast house dust	Coke dust	Premix
Fe_2O_3 (%)	89.33	89.80	37.49	2.84	64.47
CaO (%)	0.52	0.47	14.17	1.28	14.61
SiO_2 (%)	6.19	6.00	8.20	7.79	9.88
Al_2O_3 (%)	0.53	0.48	3.12	4.04	3.39
MgO (%)	2.60	2.41	1.65	0.17	2.38
SO_3 (%)	0.15	0.13	2.02	4.58	1.15
C (%)	0.22	0.12	36.96	82.70	8.96
ZnO (ppm)	-	-	3,323	205	879
Na_2O (ppm)	1 585	1 648	1 697	919	5 479
PbO (ppm)	-	-	470	200	68
K_2O (ppm)	832	790	5 405	3 298	3 839
MnO (ppm)	523	478	2 315	157	11 900
V_2O_5 (ppm)	1 180	1 252	2,537	425	7 529
TiO_2 (ppm)	1 283	1 468	3,627	5 500	3 560
P_2O_5 (ppm)	370	349	1 163	2 231	3 071

Table 6. Chemical composition of side streams used to produce ettringite-based binder briquettes (Reprinted under CC BY 4.0 license from Publication II © 2022 Authors).

Element	Briquette fines	Desulfurization scrap	Mill scale	Steel scrap	Rapid cement	GGBFS cement
Fe_2O_3 (%)	54.25	36.99	95.70	69.54	3.66	0.54
CaO (%)	21.49	37.80	-	11.57	63.03	38.06
SiO_2 (%)	12.78	11.87	0.73	8.46	18.40	34.83
Al_2O_3 (%)	3.53	1.57	0.13	3.12	4.43	9.68
MgO (%)	2.89	0.17	0.08	2.28	2.46	10.56
SO_3 (%)	2.04	6.01	0.04	0.49	5.26	3.03
C (%)	11.03	2.31	0.19	0.92	0.87	0.21
ZnO (ppm)	338	-	685	623	514	35
Na_2O (ppm)	8 422	3 530	734	5 172	10 140	6 309

Element	Briquette fines	Desulfurization scrap	Mill scale	Steel scrap	Rapid cement	GGBFS cement
PbO (ppm)	48	-	-	-	109	-
K_2O (ppm)	4 250	910	-	1 329	10 190	7 472
MnO (ppm)	5 527	3 620	8 803	14 250	476	2 602
V_2O_5 (ppm)	3 518	3 510	201	6 114	-	-
TiO_2 (ppm)	3 924	6 570	214	3 048	2 177	14 090
P_2O_5 (ppm)	1 345	1 050	409	2 592	962	34

Table 7 shows the chemical composition of the side streams used in producing self-reducing and slag-forming briquettes to be tested for their suitability for EAF use.

Table 7. Chemical composition of side streams used in producing EAF briquettes (Adapted, with permission, from Publication III © 2021 Wiley-VCH GmbH).

Material	Al_2O_3	CaO	Cr_2O_3	MgO	MnO	P_2O_5	S	SiO_2	Fe_2O_3
Ladle furnace slag 1	8.27	46.65	0.04	11.74	1.98	0.50	0.38	27.52	1.42
Ladle furnace slag 2	11.23	50.61	0.17	9.83	0.56	0.48	1.22	21.18	2.08
Mixed residues	14.07	37.93	0.53	13.99	2.76	0.61	0.63	14.82	11.84
Belt conveyor fines	0.21	90.08	1.06	0.99	1.45	0.33	0.21	2.97	1.75
Oxy-cutting fines	0.17	1.29	0.65	0.36	0.81	0.53	0.18	1.06	92.72
Combustion chamber dust	1.91	9.30	1.28	1.95	3.45	0.63	0.19	4.38	64.09
Grinding sludge	1.06	0.15	1.73	0.10	0.32	0.43	0.08	3.57	92.09
Ferromanganese carbon dust*	1.89	5.61	-	3.38	58.81	0.06	-	9.65	2.67

* Rest in wt.%: 9.86 K_2O; 3.90 Na_2O; 0.99 Cl.

X-ray diffraction (XRD) using Rigaku SmartLab 9 kW, employing 2θ in the range between 5 to 120º and a step of 0.02º, was used to determine the mineralogical phases of the side streams used to produce the briquettes. Samples were scanned under conditions of 40 kV and 135 conditions. Rigaku integrated X-ray powder diffraction software PDXL 2.6 was used to analyze the diffraction patterns and determine the phases. Table 8 shows the detected phases in the side streams used to produce reference and LSG briquettes.

Table 8. Detected phases in side streams used to produce reference and LSG briquettes (Reprinted under CC BY 4.0 license from Publication II © 2022 Authors).

Side stream	Detected phases
Coarse pellet fines	Hematite – Magnetite – Quartz
Fine pellet fines	Hematite – Magnetite – Quartz
BF stock/cast house dust	Hematite – Magnetite and/or Wüstite – Quartz
Premix	Hematite – Magnetite – Wüstite – Quartz

Side stream	Detected phases
Briquette fines	Hematite – Calcite – Magnetite- Wüstite
Desulfurization scrap	Iron- Portlandite – Calcite – Magnetite – Quartz
Mill scale	Magnetite – Wüstite – Hematite – Iron
Steel scrap	Wüstite – Magnetite – Quartz – Calcite

3.2.5 Briquette-making from side streams

In Publication II, side streams were used to produce two types of briquettes: reference briquettes and LSG briquettes. Reference briquettes were produced using ordinary Portland rapid cement and GGBFS with a ratio of 50:50. These briquettes were used as a reference against which to assess the performance of LSG binder. Reference briquettes contained 12.6% binder on a dry mass basis. The material constituting the side streams of the recipe used for all briquette-making is shown in Table 9. Briquette components were dry-mixed in a lab bowl using a mixer until a homogeneity was reached. Water was added gradually afterwards, and mixing continued until a wet paste was obtained. Water content made up 9.5% of the briquette on a dry mass basis.

Table 9. Side stream material mixtures used to produce the reference and LSG briquettes (Reprinted under CC BY 4.0 license from Publication II © 2022 Authors).

Material	Content (wt.%)
Coarse pellet fines	7.11
Fine pellet fines	19.88
Cast house dust	4.01
Coke dust	4.94
Premix (60:40 steel scrap and BF top dust)	21.99
Briquette fines	12.51
Desulfurization scrap	5.56
Mill scale	21.37
Steel scrap	2.63

LSG briquettes were produced using LSG binder from ladle slag and gypsum, employing the same approach. The content of binder in the LSG briquettes was 10, 15 and 20% of the briquette on a dry mass basis, and the briquettes produced were labelled LSG10, LSG15, and LSG20 accordingly. To produce LSG briquettes, the binder was first prepared by dry mixing gypsum and ladle slag powder. The LSG binder uses ladle slag and gypsum as precursors with a ladle slag-to-gypsum ratio of 70:30, which was the optimized ratio (Nguyen et al., 2019). The selected water-

to-binder ratio was 0.45 to facilitate effective and fast hydration in the LSG binder. Citric acid was dissolved in water to produce a 1 wt.% citric acid solution prior to its use to activate the binder. All binder components were thoroughly mixed for 2 mins to obtain a homogenous binder. The results of ladle slag chemical analysis are shown in Table 10.

Table 10. Chemical composition (wt.%) of ladle slag measured by XRF.

	CaO	SiO_2	Al_2O_3	Fe_2O_3	MgO	SO_3	others
LS	51.0	8.3	27.9	1.1	6.3	0.8	4.6

Seven briquettes were produced as part of Publication III. BRIQ1, BRIQ3, BRIQ4, and BRIQ5 were intended to be used as self-reducing briquettes, while BRIQ2, BRIQ6, and BRIQ7 were intended to be used as slag-forming briquettes. Table 11 below shows the composition of each briquette produced to be tested for suitability for use in an EAF as part of Publication III.

Table 11. Side stream material mixtures used to produce briquettes tested for EAF use (wt.%) (Adapted, with permission, from Publication III © 2021 Wiley-VCH GmbH).

Side stream	BRIQ1	BRIQ2	BRIQ3	BRIQ4	BRIQ5	BRIQ6	BRIQ7
Grinding sludge	-	-	46.00	43.10	-	-	-
Belt conveyor fines	–	63.40				-	-
Oxy-cutting fines	36.20	-	33.80	33.80		-	-
Combustion chamber dust	35.90	-				-	-
Carbon injected	15.60	-	10.20	10.20	8.40	-	-
Ferromanganese carbon dust	-	-	-	-	69.70	-	-
$Ca(OH)_2$	-	-	-	-	2.40	-	-
Fibers	0.90	0.70	0.90	1.90	1.00	-	0.90
Starch	4.00	4.80	9.20	11.00	6.90	5.00	8.80
Water	7.40	31.10	-	-	11.70	-	2.20
Mixed residues	-	-	-	-	-	-	44.10
Ladle furnace slag_1	-	-	-	-	-	80.90	-
Ladle furnace slag_2	-	-	-	-	-	-	44.10
Sodium silicate	-	-	-	-	-	14.10	-

Based on the chemical composition of the side streams used to produce the briquettes tested in Publication III, the chemical compositions of the briquettes were calculated and are shown in Table 12.

Table 12. Chemical compositions of briquettes tested for suitability for EAF use (wt.%). Balance consists of starch, fibers, and minor elements (Adapted, with permission, from Publication III © 2021 Wiley-VCH GmbH).

Briquette	Al_2O_3	CaO	Cr_2O_3	MgO	MnO	P_2O_5	S	SiO_2	Fe_2O_3	C (Injection)
BRIQ1	0.81	4.11	0.76	0.90	1.66	0.45	0.15	2.12	61.09	16.84
BRIQ2	0.20	82.89	0.98	0.92	1.34	0.31	0.19	2.74	1.62	-
BRIQ3	0.55	0.51	1.02	0.17	0.42	0.38	0.10	2.00	73.63	10.18
BRIQ4	0.52	0.51	0.97	0.17	0.41	0.37	0.10	1.90	71.03	10.20
BRIQ5	1.49	4.48	0.00	2.67	46.37	0.05	0.00	7.61	2.11	9.50
BRIQ6	6.69	37.74	0.04	9.50	1.61	0.41	0.31	22.26	1.15	-
BRIQ7	11.40	39.88	0.32	10.73	1.50	0.50	0.84	16.22	6.27	-

A Carver lab-press and die briquetting machine, shown in Fig. 5, was used to produce the reference and LSG briquettes studied in Publication II, as well as BRIQ4 studied in Publication III. Briquetting pressure was set to 100 bar, and vibration was set to 50 Hz.

Fig. 5. A lab-press and die briquetting machine used to produce briquettes.

Reference briquettes were cured under high humidity conditions for the first two days and then cured in ambient conditions until the 28th day. LSG briquettes were cured in ambient conditions. The produced briquettes used in Publication II were of cylindrical shape with a diameter and height of 55.5 and 51.0 mm, respectively.

The physical characteristics of the briquettes studied in Publication III are shown in Table 13 below.

Table 13. Physical characteristics of briquettes studied in Publication III to be tested for their suitability for EAF use (Adapted, with permission, from Publication III © 2021 Wiley-VCH GmbH).

Briquette	Height (cm)	Apparent density (g/cm^3)	True density (g/cm^3)	Porosity (%)
BRIQ1	40.60	2.23	3.0827	27.77
BRIQ2	39.28	1.49	2.3990	37.87
BRIQ3	33.60	2.24	3.2139	30.27
BRIQ4	45.42	2.14	3.1223	31.41
BRIQ5	27.58	1.62	2.7809	41.71
BRIQ6	44.17	2.33	2.9307	20.55
BRIQ7	34.08	1.88	2.8929	35.07

4 Methods and testing

This research focused on minimizing the emissions and increasing recycling within iron- and steelmaking. To achieve this target, the research focused on studying the influence of hydrogen on the reduction behavior of acid iron ore pellets in simulated BF conditions. Moreover, the research focused on producing briquettes with enhanced chemical, thermal, and mechanical characteristics to minimize fine particles generation and sustain adequate levels of furnace permeability during furnace operation. Compression and drop tests were performed to assess the mechanical properties of the newly produced briquettes. Swelling, chemical reactions, reduction, and evolved gases were assessed utilizing a blast furnace simulator (BFS) and TGA coupled with an MS.

4.1 Briquettes' mechanical properties testing

4.1.1 Compression strength (related to Publication II and Publication III)

To assess the briquettes' compression strength, compression tests were carried out according to BS ISO 4700:2007 using a 100 kN Zwick/Z100 machine, shown in Fig. 6 (British Standards Institution, 2015). Specimens were placed between two parallel platens, and the compression speed was set to 10 mm/min. The test concluded either when the load fell to less than 50% of the maximum load recorded or when the gap between the two parallel platens became less than 50% of the specimen height. Compression strength can be determined based on the following relation:

$$\sigma_c = \frac{F}{A}, \tag{16}$$

where:

- σ_c is the compression strength in MPa;
- F is the force at which the briquette suddenly fails in N; and
- A is the cross-section area of the tested briquette in mm^2.

Fig. 6. Briquette placed between two parallel platens in 100 kN Zwick/Z100 machine used to perform compression strength tests for briquettes.

4.1.2 Drop damage resistance (related to Publication II and Publication III)

Drop damage resistance assessment of the briquettes was carried out to measure the briquettes' ability to withstand handling and charging to the furnace. In drop damage resistance tests of reference and LSG briquettes studied and presented in Publication II, testing took place after 2, 7, and 28 days of curing. In each test, a sample was repeatedly dropped from a height of 1 m into a top-opened steel box. After each drop, the briquette was weighed using a scale. The procedure was repeated until the mass that had disintegrated as a result of drops exceeded 50% or the briquette had survived 50 drops while retaining more than 50% of its original mass. The drop damage resistance was expressed as the number of briquette drops before the test was completed.

The briquettes tested and presented in Publication III were tested following the same procedures; however, the curing period and the height from which the briquettes were dropped varied. The briquettes to be used in EAF were tested after prolonged curing (2 years) by dropping them from a height of 2 m into the steel box. BRIQ4 was tested for early strength development by dropping it from a height

of 1 m after 2 days of curing and 5 m after 7 days of curing. Ferroalloys (FA) used in operating EAFs were obtained and tested following the same procedures to provide a reference against which the briquettes' drop damage resistance could be assessed.

In Publication II, the drop height was chosen to obtain results comparable to those in the literature. In Publication III, the testing heights were chosen in an attempt to simulate the height from which briquettes would drop into an operating EAF.

4.2 High temperature testing

4.2.1 Reduction of pellets in BFS (related to Publication I)

Multi-point vertical probing (MPVP) measurements were carried out at Dillinger BF, BF-4. Six probes were radially distributed across the top of furnace from the center position to the wall of the furnace and were allowed to descend from the top downwards. While descending, the probes were used to measure the content of CO, CO_2, and H_2. Information regarding the position of the probe and its movement path during descent can be found elsewhere (Lecacheux et al., 2011) . In the current research, average condition measurements were utilized to study the influence of the H_2-H_2O content in reducing gas on the reduction of acid iron ore pellets. Thermodynamic software HSC chemistry 8.1 was used to estimate the content of H_2O in the reducing atmosphere because H_2O content was not directly measured by the descending probes. H_2O content was calculated such that the oxygen equilibrium partial pressure was equal for H_2O and CO_2 formation reactions in both reducing atmospheres. Therefore, CO and H_2 had the same reduction potential during the process. Nitrogen was then assumed to constitute the remainder of the gas composition.

CO and H_2 gas utilization were calculated using equations (17) and (18):

$$\eta_{CO} = \frac{CO_2}{CO + CO_2} \times 100, \tag{17}$$

$$\eta_{H_2} = \frac{H_2O}{H_2 + H_2O} \times 100, \tag{18}$$

where η_{CO} and η_{H_2} are gas utilization numerical indices. The reduction conditions for both reducing atmospheres are shown in Bauer-Glaessner phase stability diagrams in Fig. 7. Furthermore, data from HSC Chemistry software version 8.1.

was used to draw the line depicting Boudouard reaction, which was superimposed on Fe-O-C diagram.

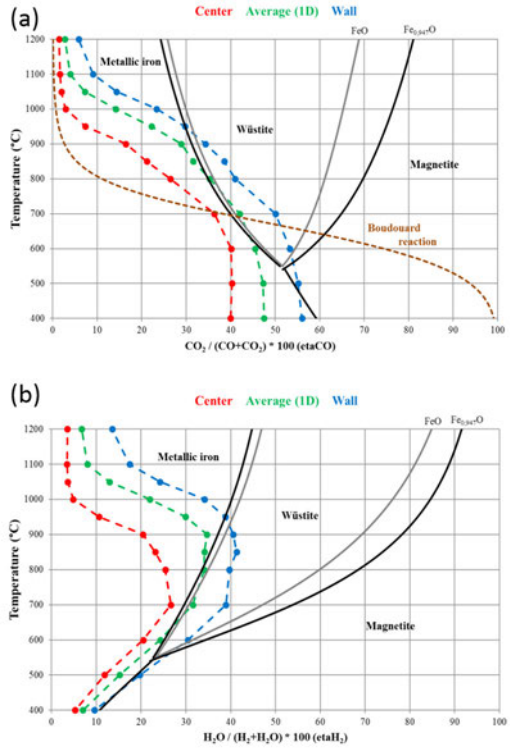

Fig. 7. Reduction conditions at different positions of the blast furnace illustrated on Bauer-Glaessner diagrams using ηCO (a) and ηH_2 (b).

In the case that reduction time is sufficient, the most stable phase shown on the diagram should be reached. The content of the reducing gas and the oxygen partial pressure are shown in Table 14.

Table 14. Reducing gas content during reduction experiment at average conditions (Modified under CC BY-NC-ND 4.0 license from Publication I © 2021 The Iron and Steel Institute of Japan).

		$CO-CO_2-N_2$ gas				$CO-CO_2-H_2-H_2O-N_2$ gas					
Temp	#	CO	CO_2	N_2	#	CO	CO_2	H_2	H_2O	N_2	p_{O_2}
(°C)		(Vol.%)	(Vol.%)	(Vol.%)		(Vol.%)	(Vol.%)	(Vol.%)	(Vol.%)	(Vol.%)	(atm)
700	1	28.02	20.31	51.67	6	26.39	19.13	3.98	1.84	48.66	3.00E-22
800	2	31.81	17.34	50.84	7	29.64	16.16	4.50	2.33	47.37	1.14E-19

		$CO-CO_2-N_2$ gas				$CO-CO_2-H_2-H_2O-N_2$ gas					
Temp	#	CO	CO_2	N_2	#	CO	CO_2	H_2	H_2O	N_2	p_{O_2}
(°C)		(Vol.%)	(Vol.%)	(Vol.%)		(Vol.%)	(Vol.%)	(Vol.%)	(Vol.%)	(Vol.%)	(atm)
900	3	34.69	14.11	51.20	8	31.95	12.99	5.17	2.75	47.15	1.39E-17
1000	4	41.43	6.84	51.73	9	38.09	6.29	6.29	1.77	47.56	2.14E-16
1100	5	46.01	1.89	52.10	10	42.52	1.74	6.98	0.60	48.15	6.31E-16

In this work, isothermal reduction experiments were carried out using a modified BFS. The BFS consisted of a 95 mm inner diameter-tube furnace. Several gases can be used in a BFS, including CO, H_2, CO_2, and N_2. Additionally, it was possible to introduce H_2O into the furnace through a pumping system that was connected to the apparatus. The apparatus was connected to a computer system that could be used to set pre-determined reducing program parameters, such as gas composition, volume flow rate, and temperature. A weight scale at the top of the furnace was used to suspend the basket containing the sample and continuously record the weight at fixed intervals. The apparatus setup is illustrated in Fig. 8.

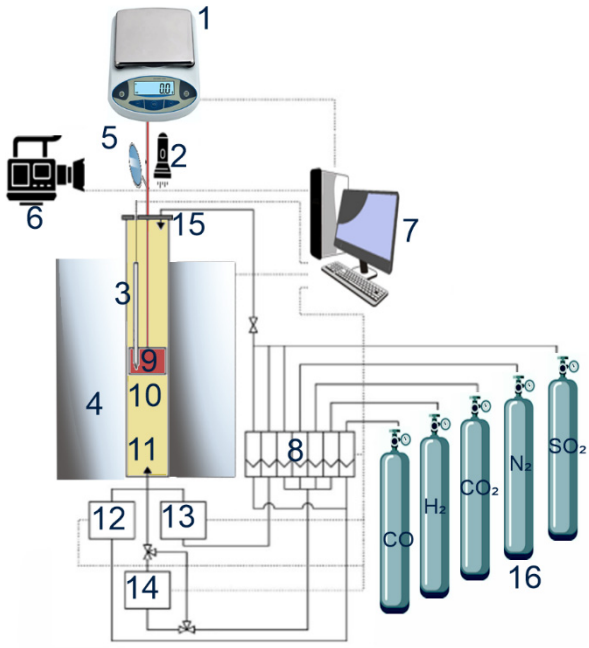

Fig. 8. BFS apparatus setup used in isothermal and dynamic reduction tests. (1) Scale, (2) light torch, (3) thermocouple, (4) electrically heated furnace, (5) mirror, (6) video camera, (7) computer system, (8) mass flow control, (9) sample basket, (10) reduction tube, (11) water pump, (12) sulfur generator, (13) potassium generator, (14) gas inlet, (15) transparent lid and cooling gas inlet, and (16) gas cylinders (Reprinted under CC BY 4.0 license from Publication II © 2022 Authors)

In each isothermal reduction test, a total of 30 pellet pieces, weighing 100 ± 0.1 grams, were used. The pellet pieces were placed in a single layer in a basket to avoid hindering the gases from rising through the basket samples. The basket was introduced to the furnace and freely suspended through the weight balance at the top. The weight balance continuously recorded the combined weight of the sample and basket at 10-second intervals. The furnace was then heated to the target temperature using a flow of nitrogen gas, which was introduced to the furnace at a rate of 15 l/min (NTP). A temperature fluctuation of ± 10 °C within the furnace was considered acceptable. The reduction program was started afterward using the furnace software on the computer unit; the reducing gases were introduced to the furnace according to the pre-determined reduction program, as shown in Table 14. The reduction phase was 300 minutes, during which the total gases' flow rates were

set to 15 l/min (NTP). After the completion of the reduction phases, nitrogen was introduced to the furnace at a rate of 10 l/min (NTP) to cool the samples in an inert atmosphere, avoiding the possibility of the samples' re-oxidation.

The reduction of iron ore oxides proceed in a stepwise manner, from hematite to metallic iron, as follows:

$$3\,Fe_2O_3 + CO\ (\text{or}\ H_2) \rightarrow 2\,Fe_3O_4 + CO_2\ (\text{or}\ H_2O), \tag{19}$$

$$Fe_3O_4 + CO\ (\text{or}\ H_2) \rightarrow 3\,FeO + CO_2\ (\text{or}\ H_2O), \tag{20}$$

$$FeO + CO\ (\text{or}\ H_2) \rightarrow Fe + CO_2\ (\text{or}\ H_2O). \tag{21}$$

The reduction degree is estimated according to ISO 7215:2015 standard (ISO 7215: 2015, 2015), employing the following equation:

$$R = \frac{m_1 - m_2}{m_1(0.430\,w_2 - 0.111\,w_1)} \times 10^4\,, \tag{22}$$

where m_1 is the mass of the pellet sample prior to reduction in grams, m_2 is the mass of the sample after reduction in grams, w_1 is the iron (II) oxide mass percentage in the sample before reduction, and w_2 is the total iron mass percentage in the sample before reduction.

4.2.2 Briquettes' reduction and swelling (related to Publication II and Publication III)

In Publication II, the same BFS apparatus was used to study the reduction of briquettes. However, the reduction program shown in Table 15 was employed to test the reference and LSG briquettes used in Publication II. The employed temperature and gas profiles in the reduction program were based on an ISO standard test for BF ironmaking (British Standards Institution, 2007b).

Table 15. BFS gas and temperature profile employed in LSG briquettes reduction and swelling tests (Reprinted under CC BY 4.0 license from Publication II © 2022 Authors).

Time (min)	Temperature (°C)	N_2 (%)	CO (%)
0 → 120	25 → 950	100	0
120 → 135	950	100	0
135 → 375	950	60	40

To calculate the briquette swelling, briquette shape was assumed to be a perfect cylinder. The total swelling was calculated as the difference between the final and initial volume of the briquette, using the following equation:

$$\Delta V_{briquette} = \frac{A_f h_f - A_i h_i}{A_i h_i} \times 100\%\,, \tag{23}$$

where A_f is the final top surface area of the briquette after reduction, h_f is the final briquette height after reduction, A_i is the initial top surface area of the briquette before reduction, and h_i is the initial briquette height before reduction.

During reduction, a top view of the briquette was recorded by a video camera, capturing the dimensions of briquette's top surface. The briquette's swelling was assumed to be uniform (as the top surface area increased, reaching the final area, the briquette height increased proportionally, reaching the final height). Swelling was then calculated similarly based on equation (23).

In Publication III, a full briquette (full-sized, as-produced briquette without prior cutting) of each recipe was investigated through the same apparatus. Nitrogen was used to purge the reduction chamber for 5 minutes at a flow rate of 10 l/min. The sample was then heated from room temperature to 1100 °C, with reducing gases introduced as per the reduction program shown in Table 16. The flow of reducing gases was maintained at 15 l/min. After reaching the desired temperature, the sample was allowed to cool through a flow of nitrogen at 10 l/min.

Table 16. Gas composition during dynamic reduction in the reduction tube furnace (Adapted, with permission, from Publication III © 2021 Wiley-VCH GmbH).

Gas	N_2	CO	CO_2	H_2
(%)	31.00	50.00	15.00	4.00

4.2.3 Briquettes' thermogravimetric analysis and mass spectrometer (related to Publication II and Publication III)

In Publication II, thermogravimetric analysis (TGA) was used to study the influence of substituting Portland cement with LSG binder. Thermogravimetry assesses the thermal stability of material against temperature and time. Netzsch STA 449F3 coupled with Quadrupole Mass Spectrometer (QMS) 403 Aëolos Quadro was used to carry out TGA. An MS was used to analyze the resulting evolving gases during sample heating. Commercially available software, Netzsch

Proteus 6.1, was used to analyze the results. The sample used was a 1 cm^3 cubic briquette piece cut from a briquette from each recipe using a saw. The sample weighed around 4 g and was used without subsequent grinding. During analysis, the sample was heated from room temperature to 1600 °C with a heating rate of 30 °C/min and Ar gas flowing at 40 ml/min. Similar procedures were followed to test the briquette specimens investigated in Publication III. However, the target temperature was set to 1300 °C with a heating rate of 5 °C/min and Ar flow of 60 ml/min.

4.2.4 Melting trials (related to Publication III)

Melting trials were carried out for two briquette types studied in Publication III using a chamber furnace shown in Fig. 9. The furnace employed in the melting trials was a basic chamber furnace by Nabertherm: 10 x U-shaped $MoSi_2$ (molybdenum disilicide), heating elements manufactured by Kanthal with a maximum temperature of 1900ºC, and B-type thermocouple. Chamber size was 150 (height) x 150 (width) x 300 (depth) mm. Controls were obtained from Eurotherm. In the melting trial, the briquettes' interaction with molten slag was observed, and their behavior when in contact with slag was studied. Each briquette studied was intended to be used at a different EAF; therefore, the slag used in each melting trial was obtained from the same EAF at which the corresponding briquette was intended to be used. Prior to the melting trials, slag was ground and chemically analyzed. Slag was then placed in a platinum crucible (Approximately 5 cm in diameter) and was roasted overnight in air to ensure that iron was oxidized. During the melting trials, the platinum crucible with 40 g of slag was placed in the chamber furnace, and the temperature was set to 1550 °C, which resulted in slag melting. After the slag was melted, a 1 cm^3 cubic piece of the briquette was placed on top of the molten slag. A video recording camera was placed in front of the chamber furnace door to capture the melting process of the briquette. The furnace door was opened at short intervals to observe the interaction between the slag and the briquette piece until the briquette was completely molten. To verify the furnace temperature changes during melting trials, the furnace was heated to 1550 °C. In a period of 1 minute and 5 seconds, the furnace door was opened three times for 10 seconds each, resulting in a temperature drop from 1550 °C to 1480 °C. The temperature drop was 4.66% of the starting temperature, which was considered acceptable.

The chemical compositions of the two slag types used in melting trials were determined by XRF and are shown in Table 17 below.

Table 17. Chemical composition of plant No.1 and plant No.2 slag (wt.%), determined through XRF (Adapted, with permission, from Publication III © 2021 Wiley-VCH GmbH).

	Na_2O	MgO	Al_2O_3	SiO_2	SO_3	K_2O	CaO	Cr_2O_3	MnO	Fe_2O_3
Plant 1 slag	0.21	5.70	14.58	14.9	0.17	0.02	22.18	2.57	4.33	29.41
Plant 2 slag	0.53	3.36	5.93	29.17	0.31	0.05	15.49	1.85	3.49	27.36

Fig. 9. Chamber furnace used to carry out melting trials for briquettes assessed for their suitability for EAF use.

4.2.5 Dilatometry testing (related to Publication III)

To study the softening and melting behavior of briquettes, an optical dilatometer was used. The optical dilatometer consisted of a horizontal furnace (inner diameter of 31 mm) with a computer-connected camera placed in alignment with the sample, as shown in Fig. 10. The computer-connected camera was able to capture an image of the sample at 5 °C intervals. The sample was heated at a rate of 5 °C/min to 1510 °C in nitrogen gas flowing at 3.5 l/min. The 1 cm^3 samples were cut from each briquette and weighed around 4 g. As the samples' size was relatively large, a

special sample holder with side edges was made and used to prevent the sample melt from overflowing to the sides. The sample holder was made of alumina magnesia (aluminum oxide–magnesium oxide) spinel. Spinel powder from industry was used. Particles larger than 1 mm were removed by sieving. The powder was mixed with water, poured in a mold, allowed to harden for two days, removed, and heat treated at 1200ºC.

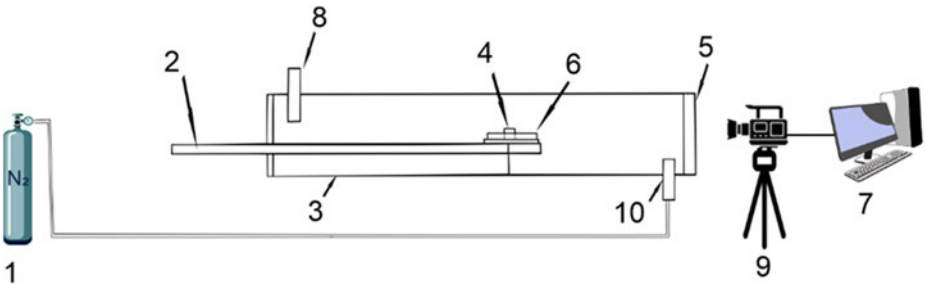

Fig. 10. Dilatometer apparatus used in the tests. 1. Nitrogen gas cylinder 2. Push rod with thermocouple 3. Water-cooled stainless steel tube furnace 4. Sample 5. Quartz glass 6. Sample holder 7. Computer system 8. Gas outlet 9. Camera 10. Gas inlet (Adapted, with permission, from Publication III © 2021 Wiley-VCH GmbH).

4.3 X-Ray diffraction

To determine the crystalline phases of the samples tested, Rigaku SmartLab 9 kW was used. The range of 2θ employed was 5–130° in Publication I and 5–120° in Publication II with a 0.02° step. Scanning speed was set to 4 degree/min at 40 kV and 135 mA. Rigaku-integrated X-ray powder diffraction software PDXL 2.6 was used to analyze the diffraction patters obtained. In Publication I, three pellets from each reduction experiment, as well as three unreduced pellets, were ground to prepare XRD samples. In Publications II and III, side streams were ground to prepare XRD samples. Moreover, briquettes were ground to investigate mineralogical phases prior to and after reduction.

4.4 Microscopy

To study the morphology and cross section areas of the tested specimens, a field emission scanning electron microscope (FESEM; Zeiss Ultra Plus, Carl Zeiss SMT AG, Germany) was used. The FESEM was attached to an energy-dispersive X-ray

spectroscope (EDS) to study the samples' chemical composition. In Publication I, two sets of samples were prepared. In the first set, the pellet was symmetrically cut into two pieces. The pieces in the first set were used to study the surface morphology of the unreduced and reduced pellets. The pellet piece was fixed on a sample holder using carbon tape and was Pt coated. An acceleration voltage of 5 kV was used when studying the samples. The second set of specimens was embedded in resin, vacuum impregnated, and allowed to harden overnight in an oven. Each sample was ground and polished in order to examine the cross-section area. Synthetic diamond was used as an abrasive. Grinding took place in two steps: first, plane grinding using #500 grit size, and second, fine grinding using a 9 μm particle size. Polishing took place in two steps: first, using a 3 μm particle size, and second, using a 0.25 μm particle size. Polished samples were Au coated and were used to study the cross-section area of the unreduced and reduced samples through an Olympus BX51 light optical microscope (LOM). Moreover, a laser scanning confocal microscope (LSCM; Keyence, VK-X100K/X200K) equipped with a motorized X-Y stage was used to obtain a mosaic cross-section area of unreduced and reduced pellets. The mosaic images of the cross-section area were assembled through an image assembling application (VK-H1XJ).

Similarly, two different specimens from Publication III were examined. The first set consisted of reduced briquettes, which were utilized to study the cross-section area. Specimens were mounted in epoxy, cut, and polished using Struers LaboPol-6 prior to investigate using FESEM. Moreover, EDS was used to construct an elemental map of the specimens. The second set of specimens were examined for their morphology without prior polishing.

4.5 Porosity and surface area changes

To determine the porosity of pellets studied in Publication I, their skeletal and envelope densities were first determined. Skeletal density (ρ_S) is defined as the mass of the sample divided by its volume, excluding the volume of open pores. Skeletal density was determined using an AccuPyc II 1340 gas pycnometer with a 10 cm^3 sample chamber, employing helium as a displacement gas. The skeletal densities of three pellets were determined at a time. To determine a pellet's envelope density (ρ_e), ImageJ image analysis software was used to determine the pellet's equivalent circular diameter as follows:

$$D_a = 2\sqrt{\frac{A}{\pi}}, \tag{24}$$

where A is the pellet's projected area.

The steps followed to obtain a pellet's equivalent circular diameter using ImageJ are shown in Fig. 11. Each pellet's envelope volume was then obtained based on the pellet's equivalent circular diameter. The pellet's mass and volume was then used to determine the pellet's envelope density (ρ_e). Pellet porosity (ε) was calculated as follows:

$$\varepsilon = \frac{\rho_S - \rho_e}{\rho_S} \times 100, \quad (25)$$

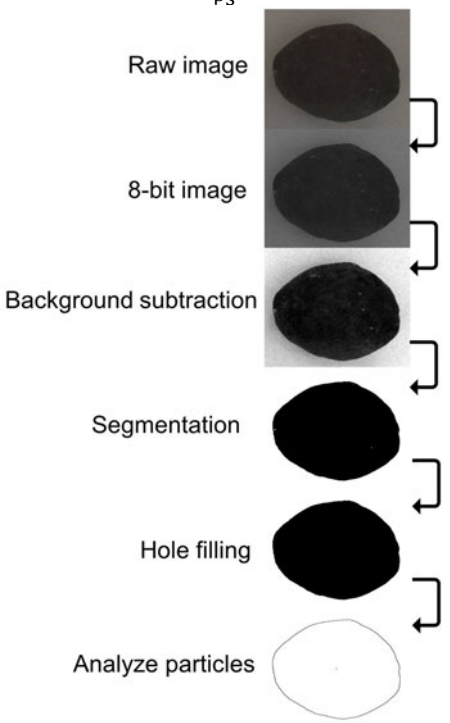

Fig. 11. Pellet image processing to obtain the pellet's projected area (Modified under CC BY-NC-ND 4.0 license from Publication I © 2021 The Iron and Steel Institute of Japan).

This procedure was repeated three times using three different pellets from each reduction experiment, and the density was estimated to be the average of the three measurements.

Similarly, the porosities of briquettes studied in Publications II and III were calculated based on ρ_e envelope density and ρ_s skeletal density. Skeletal density was determined with the gas pycnometer using three 1 cm^3 cubic samples cut from

briquettes. The envelope density of briquettes was determined based on the geometry of the briquettes and their mass, assuming they were perfect cylinders.

The surface area of pellets studied in Publication I was obtained using a surface area and porosity analyzer, Micromeritics ASAP 2020 (Micromeritics, USA). The specific surface area was determined based on information regarding the nitrogen physisorption isotherms. The Brunauer-Emmett-Teller (BET) equation was used to calculate the surface area.

The methods and tests used in this thesis are summarized in Table 18.

Table 18. Summary of methods and analysis carried out in the thesis.

Methods	Publication I	Publication II	Publication III
Pellets samples studied	✓		
Briquettes samples studied		✓	✓
Material XRF	✓	✓	✓
Material XRD	✓	✓	✓
SEM-EDS	✓	✓	
Density and voids	✓	✓	✓
Moisture content		✓	✓
TGA-MS		✓	✓
BFS	✓	✓	✓
Dilatometry			✓
Melting trials			✓
Compression strength		✓	✓
Drop damage resistance		✓	✓

5 Results and discussion

5.1 Influence of H2 and H2O on acid pellets' microstructure and reduction

Isothermal reduction tests were carried out with varying temperature profiles and reducing gas compositions, similar to the conditions of a BF. Temperature and gas profiles were based on measured data obtained from an operating BF, which gives more realistic results than standard testing methods. Two gas profiles were used in this study: the first gas profile consisted only of CO-CO_2-N_2, while in the second gas profile, CO and CO_2 were partially replaced with equivalent content of H_2-H_2O in terms of reduction potential. The temperature and gas atmosphere were determined at the wall, center, and intermediate points of the BF. The BET surface area, porosity, and swelling of tested ores were assessed to study the influence of varying H_2 and H_2O content on the reduction behavior.

The reduction degrees obtained from the BFS reduction of pellets at temperatures of 700, 800, 900, 1000, and 1100 °C are shown in Fig. 12, Fig. 13, Fig. 14, Fig. 15, and Fig. 16, respectively. Under each reduction curve, the SEM image of the outer surface of corresponding reduced pellet is depicted. It is clear that the reduction degrees are in good agreement with the Bauer-Glaessner diagram. Pellets reduced at 700 °C in CO-CO_2-H_2-H_2O-N_2 gas appear to have a higher reduction rate and extent and were mainly reduced to wüstite, while pellets reduced in CO-CO_2-N_2 gas appear to have some unreduced magnetite. At 800 °C, pellets reduced in CO-CO_2-H_2-H_2O-N_2 gas still showed the same degree of reduction, with no improvement compared to pellets reduced at 700 °C in the same atmosphere. On the other hand, pellets reduced at 800 °C in CO-CO_2-N_2 gas achieved a comparable reduction rate and extent to those reduced in CO-CO_2-H_2-H_2O-N_2. At 900 °C, pellets reduced in CO-CO_2-H_2-H_2O-N_2 gas exhibited a higher reduction extent, showing that more metallic iron would be formed compared to pellets reduced in CO-CO_2-N_2 gas. At 1000 °C, CO-CO_2-H_2-H_2O-N_2 gas has a clear advantage, with a significantly increased reduction rate and extent compared to pellets reduced in CO-CO_2-N_2 gas. Pellets reduced at 1100 °C in both atmospheres achieved virtually complete reduction, with pellets reduced in CO-CO_2-H_2-H_2O-N_2 gas having a higher reduction rate. Pellets achieved a higher reduction extent and rate with increased temperature.

Moreover, the SEM images shown in Fig. 12 show that the surface of the pellets is composed of small aggregates of varying size. The size of the aggregates for pellets reduced in CO-CO_2-H_2-H_2O-N_2 gas appears to be smaller than for those reduced in CO-CO_2-N_2 gas. This observation is in good agreement with the BET surface area measurements shown in Fig. 21, as smaller aggregate size equates to a higher surface area. Fig. 13 shows that although reduction degree is somewhat similar between pellets reduced in both reducing atmospheres at 800 °C, the morphology of pellets reduced in CO-CO_2-H_2-H_2O-N_2 gas appears to have a more continuous solid structure compared to pellets reduced in CO-CO_2-N_2 gas. This is in good agreement with the porosity and surface area drop for pellets reduced at 800 °C in CO-CO_2-H_2-H_2O-N_2 gas, as shown in Fig. 19. Pellets reduced at 1000 °C, as shown in Fig. 15, appear to have very different morphology compared to pellets reduced at 900 °C, which are shown in Fig. 14. Pellets reduced in both reducing gases at 1000 °C appear to have developed an elongated semi-fibrous structure, which contributes to the surface area increase at 1000 °C compared to 900 °C, as shown in Fig. 19. At a temperature of 1100 °C, pellets reduced in CO-CO_2-N_2 gas appear to have formed a net-like structure. On the other hand, pellets reduced in CO-CO_2-H_2-H_2O-N_2 gas appear to have formed impermeable layer as a result of grains sintering. However, upon further magnification, the impermeable layer appears to be torn by multiple radial fissures along the surface. Such fissures were previously reported in the literature at a lower temperature (Matthew & Hayes, 1990). The radial fissures may have been the result of the buildup of gas pressure from the reduction process inside the pellets, which escapes the sintered surface of the pellet, resulting in the obvious tears at the surface, as shown in Fig. 15c.

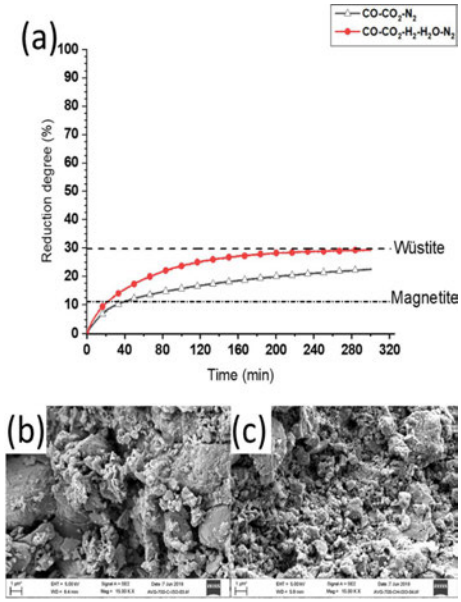

Fig. 12. Reduction curves for pellets reduced at 700 °C (a), with corresponding surface SEM images in CO-CO_2-N_2 (b) and CO-CO_2-H_2-H_2O-N_2 (c) (Modified under CC BY-NC-ND 4.0 license from Publication I © 2021 The Iron and Steel Institute of Japan).

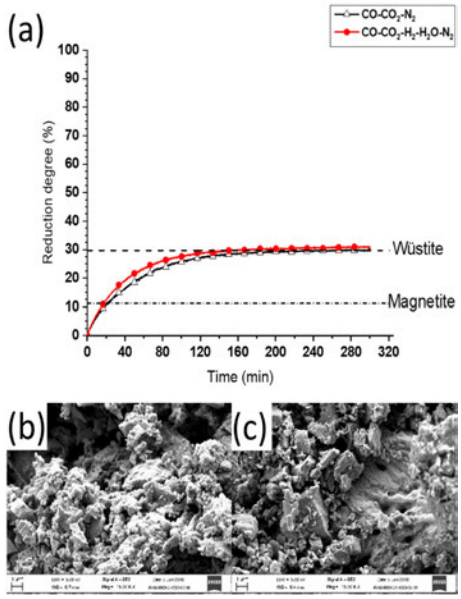

Fig. 13. Reduction curves for pellets reduced at 800 °C (a), with corresponding surface SEM images in CO-CO_2-N_2 (b) and CO-CO_2-H_2-H_2O-N_2 (c) (Modified under CC BY-NC-ND 4.0 license from Publication I © 2021 The Iron and Steel Institute of Japan).

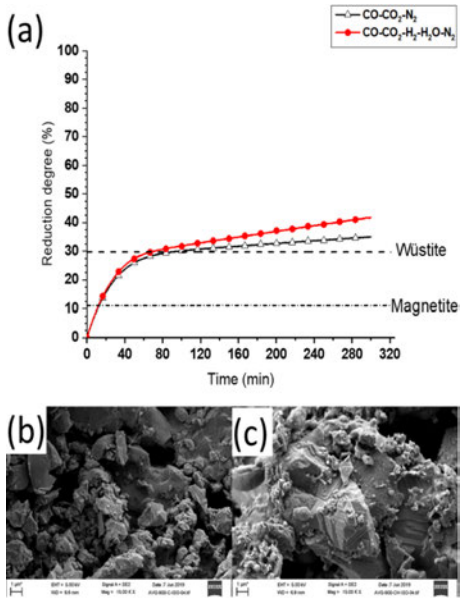

Fig. 14. Reduction curves for pellets reduced at 900 °C (a), with corresponding surface SEM images in CO-CO_2-N_2 (b) and CO-CO_2-H_2-H_2O-N_2 (c) (Modified under CC BY-NC-ND 4.0 license from Publication I © 2021 The Iron and Steel Institute of Japan).

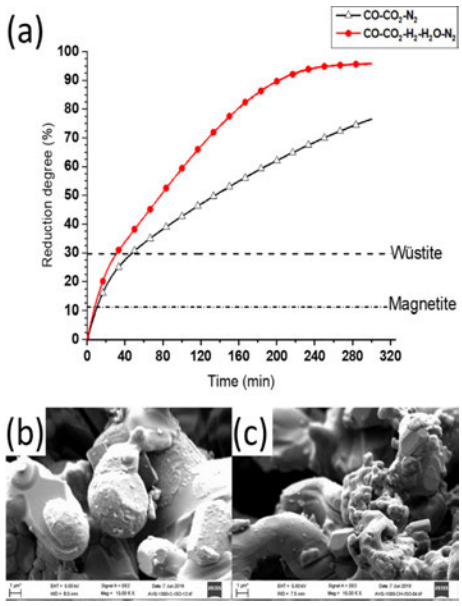

Fig. 15. Reduction curves for pellets reduced at 1000 °C (a), with corresponding surface SEM images in CO-CO_2-N_2 (b) and CO-CO_2-H_2-H_2O-N_2 (c) (Modified under CC BY-NC-ND 4.0 license from Publication I © 2021 The Iron and Steel Institute of Japan).

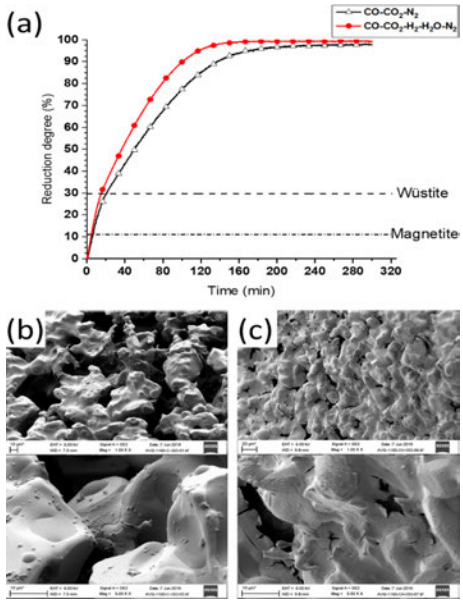

Fig. 16. Reduction curves for pellets reduced at 1100 °C (a), with corresponding surface SEM images in CO-CO_2-N_2 (b) and CO-CO_2-H_2-H_2O-N_2 (c) (Modified under CC BY-NC-ND 4.0 license from Publication I © 2021 The Iron and Steel Institute of Japan).

An increase in temperature results in an increased diffusion rate coefficient, as the movement of gas molecules become faster, which in turn supports diffusion behavior (Spreitzer & Schenk, 2019). Also, an increase in the reducing temperature results in increased porosity, which in turn results in higher reducibility of the pellets due to better access of the reducing gases to reaction sites.

Fig. 17 and Fig. 18 show mosaic cross-section areas of pellets reduced at 700, 800, and 900 °C in CO-CO_2-N_2 and CO-CO_2-H_2-H_2O-N_2 gas. No metallic iron appears to have formed at 700 °C for pellets reduced in either of the reducing gases. From the figures, it can be seen that at 800 °C, metallic iron started to form sparsely at the periphery of the pellet reduced in CO-CO_2-H_2-H_2O-N_2 gas. Metallic iron phase appeared bright white in color, but it was highlighted in green for better visibility. On the other hand, no metallic iron formed for pellets reduced at the same temperature in CO-CO_2-N_2 gas. At 900 °C, metallic iron formed at pellets' periphery in both reducing gases. However, a significant amount of metallic iron formed in pellets reduced in CO-CO_2-H_2-H_2O-N_2 gas. It also appears that the core of the pellet remained unreduced. At 1000 °C, more metallic iron formed in pellets reduced in both reducing gases. However, the core of pellets reduced in CO-CO_2-

H_2-H_2O-N_2 gas appeared to contain greater amount of metallic iron. At 1100 °C, pellets reduced in both reducing gases appeared to have been completely reduced to metallic iron. These observations are in good agreement with the Baur-Glasener diagram.

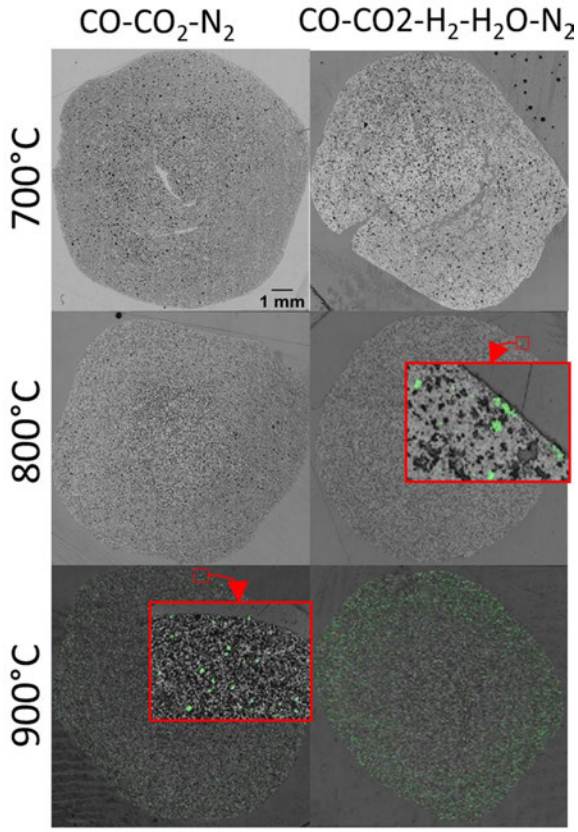

Fig. 17. Mosaic cross-section area of pellets reduced at 700, 800, and 900 °C in CO-CO_2-N_2 and CO-CO_2-H_2-H_2O-N_2 gas (Modified under CC BY-NC-ND 4.0 license from Publication I © 2021 The Iron and Steel Institute of Japan).

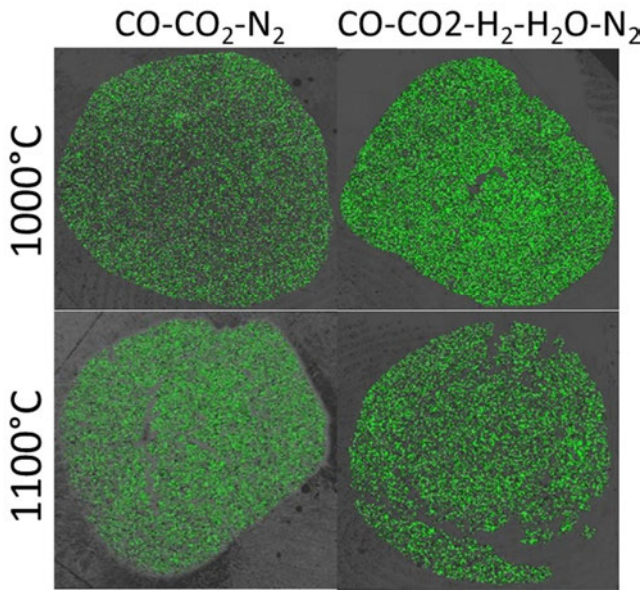

Fig. 18. Mosaic cross-section area of pellets reduced at 1000 and 1100 °C in CO-CO_2-N_2 and CO-CO_2-H_2-H_2O-N_2 gas (Modified under CC BY-NC-ND 4.0 license from Publication I © 2021 The Iron and Steel Institute of Japan).

The mineralogical phases of unreduced and reduced pellets at 700–1100 °C in both reducing gases are shown in Fig. 19. At 700 °C, pellets reduced in CO-CO_2-N_2 gas were not fully reduced to wüstite, and magnetite phase was still present. On the other hand, pellets reduced at 700 °C in CO-CO_2-H_2-H_2O-N_2 were reduced to wüstite, confirming that a CO-CO_2-H_2-H_2O-N_2 reducing atmosphere results in better reducibility, with the mixture of H_2 and CO being a superior reducing gas than CO gas alone. Also, at 1000 °C, XRD shows that metallic iron is the dominant phase in the pellets reduced in CO-CO_2-H_2-H_2O-N_2 gas, while pellets reduced in CO-CO_2-N_2 gas at the same temperature still indicate the presence of wüstite.

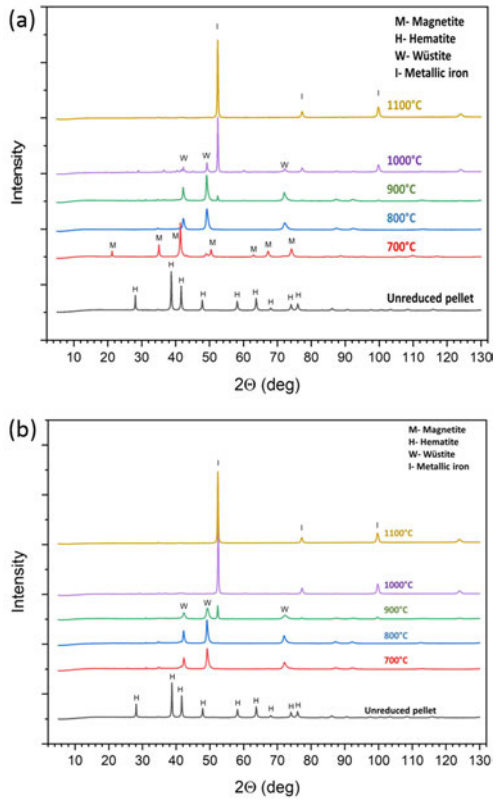

Fig. 19. Mineralogical phases of unreduced and reduced pellets in CO-CO_2-N_2 (a) and CO-CO_2-H_2-H_2O-N_2 gas (b) at a temperature of 700–1100 °C (Modified under CC BY-NC-ND 4.0 license from Publication I © 2021 The Iron and Steel Institute of Japan).

Fig. 20 shows a BFS basket containing pellets after reduction in CO-CO_2-N_2 and CO-CO_2-H_2-H_2O-N_2 gas. The surface area and porosity of pellets reduced in CO-CO_2-N_2 and CO-CO_2-H_2-H_2O-N_2 gas at 700–1100 °C are shown in Fig. 21. The figure shows that for both reducing atmospheres, as temperature increased, the porosity also increased. Moreover, the porosity of pellets reduced in CO-CO_2-H_2-H_2O-N_2 gas generally had slightly higher porosity compared to pellets reduced in CO-CO_2-N_2 gas. Also, the surface area of pellets reduced in CO-CO_2-H_2-H_2O-N_2 gas was higher than that of pellets reduced in CO-CO_2-N_2 gas. The figure also shows that pellets reduced at 700 °C had much higher surface area compared to unreduced pellets. However, as the temperature increased, BET surface area decreased, and the difference in surface area between pellets reduced in CO-CO_2-

N_2 and CO-CO_2-H_2-H_2O-N_2 gas also decreased until 1100 °C, at which point the surface area of pellets reduced in CO-CO_2-N_2 gas became slightly higher compared to those reduced in CO-CO_2-H_2-H_2O-N_2 gas. The increase in pellets' porosity was accompanied by a decrease in BET surface area, which indicates that larger but fewer pores were emerging within the pellets. The reason for this is likely the formation of dense, iron-containing, larger isolated pores (Moukassi et al., 1983). These observations are in agreement with existing literature (Ray & Ray, 2018) and the observed SEM images shown in Fig. 12, 13, 14, 15, and 16. The reducibility of iron ore is highly dependent on porosity (Hayes, 2011). As the porosity increases, the reducing gases have an easier passage into the core of the pellet, resulting in better reducibility. This may be one of the factors contributing to the fact that pellets reduced in CO-CO_2-H_2-H_2O-N_2 gas had better reducibility than those reduced in CO-CO_2-N_2 gas. However, these observations are in disagreement with some of the literature reporting that at temperatures above 1075 °C, the reduction rate decreases due to factors including ore closure and outer iron shell plastic deformation (Ray & Ray, 2018).

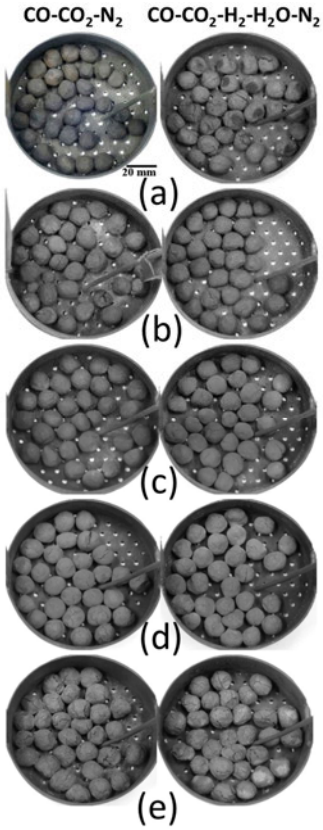

Fig. 20. BFS basket containing pellets after reduction in $CO\text{-}CO_2\text{-}N_2$ (left) and $CO\text{-}CO_2\text{-}H_2\text{-}H_2O\text{-}N_2$ (right) gas at a temperatures of 700 (a), 800 (b), 900 (c), 1000 (d), and 1100 °C (e) (Modified under CC BY-NC-ND 4.0 license from Publication I © 2021 The Iron and Steel Institute of Japan).

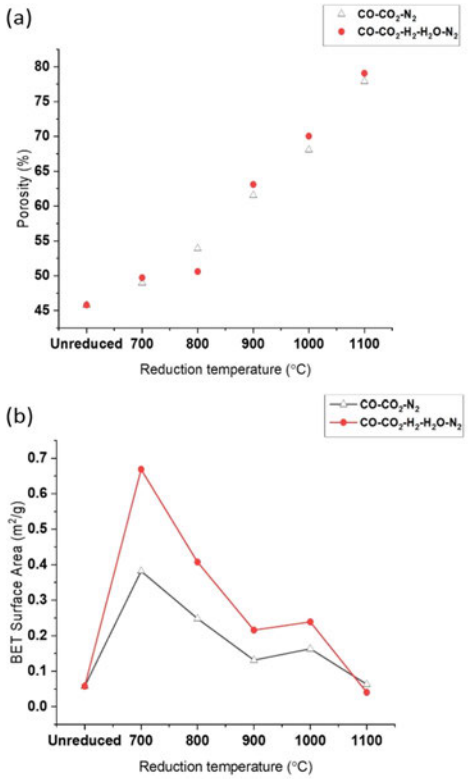

Fig. 21. Evolution of pellets' porosity (a) and surface area (b) of pellets reduced in CO-CO_2-N_2 and CO-CO_2-H_2-H_2O-N_2 gas at a temperature of 700–1100 °C (Modified under CC BY-NC-ND 4.0 license from Publication I © 2021 The Iron and Steel Institute of Japan).

5.2 Briquettes utilizing ettringite-based binder

The compression strength development 2, 7, and 28 days after the curing of reference and LSG briquettes are shown in Fig. 22. The values shown are the averages of two to three cold compression strength tests for each recipe of the briquettes. Due to the formation of C-S-H, the strength of the reference briquette increase over the 28-day curing period. During the hydration of Portland cement, 70% of C_3S reacts within the initial 28 days of curing, with the rest reacting within a year. Similarly, 90% of β-C_2S reacts during the first year of curing (Taylor, 1997). Accordingly, as more C-S-H is formed, the strength of the reference briquette is expected to increase even further over the course of a year. The reference briquette

strength is in a good agreement with values from the literature (Singh & Bjorkman, 2006).

Briquettes produced using LSG binder exhibited strength development proportional to their binder content. Briquettes produced using 15 and 20% of LSG binder exhibited high compression strength after 2 and 7 days of curing. The high early strength is attributed to ettringite ($C_3A \bullet 3C\bar{S} \bullet 32H$) formation. Ettringite is an LSG hydration product (Nguyen et al., 2019). Gibbsite (AH_3) is also formed during early hydration stages and increases briquette strength by filling the voids between formed phases, which ultimately results in improved pore structure and higher rigidity (Chang et al., 2017).

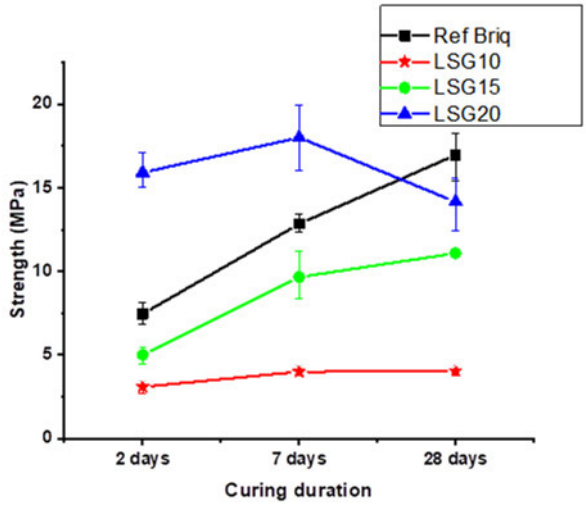

Fig. 22. Compression strength of reference and LSG briquettes produced after 2, 7, and 28 days of curing (Reprinted under CC BY 4.0 license from Publication II © 2022 Authors).

Drop test results of reference and LSG briquettes are shown in Fig. 23. After 2 days of curing, reference briquettes were able to survive 39.33 drops on average. LSG10, LSG15, and LSG20 were able to survive 5, 50, and 50 drops, respectively. It is clear that the LSG10 briquette had significantly inferior performance compared to the reference briquette after 2 days of curing. However, LSG15 and LSG20's drop damage resistance was higher compared to the reference briquette, surviving 50 drops. After 7 and 28 days of curing, the LSG10 briquette's drop damage resistance

slightly increased but remained significantly lower than that of the other tested briquettes.

The high drop damage resistance developed in briquettes containing 15 and 20% LSG binder is attributed to their high early strength development. Similar to compression strength, it is likely that the formation of ettringite during the early stages of hydration contributed to the high drop damage resistance, which was comparable to that of the reference briquette. With an increased binder content, more ettringite is formed, which is the phase responsible for the increased strength. High drop damage resistance could be particularly useful in order to avoid the breakage of briquettes during handling and moving. Also, the fact that curing took place in ambient conditions could mean significant cost savings, considering that some plants have special curing chambers for ordinary Portland cement briquettes where certain temperature and humidity levels are maintained for 24 hours following briquette production (Sundqvist Ökvist et al., 1999).

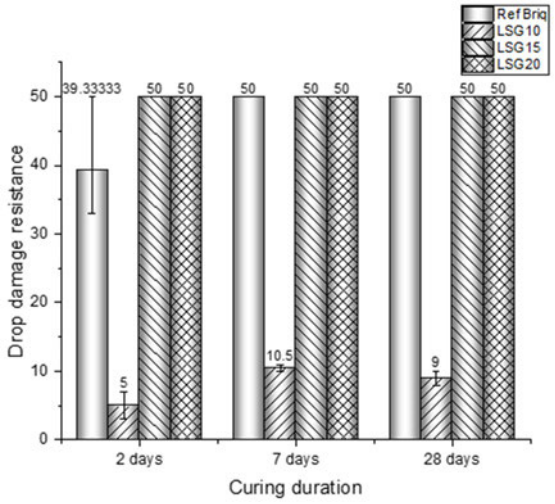

Fig. 23. Results of drop damage resistance of reference and LSG briquettes (Reprinted under CC BY 4.0 license from Publication II © 2022 Authors).

Fig. 24 shows the mass loss and swelling of reference, LSG15, and LSG20 briquettes during reduction tests in BFS. In each reduction run, a briquette was heated to 950 °C in a nitrogen atmosphere for 135 mins. Following the heating stage, CO gas was introduced in a reduction stage, which was continued for 240 mins further. During the heating stage in a nitrogen atmosphere, the reference

briquette exhibited the least mass loss, while the LSG20 briquette exhibited the highest mass loss at 5.60% and 8.56%, respectively. Below 250 °C, LSG15 and LSG20 experienced steep mass loss, which could be attributed to moisture loss and ettringite disintegration. With further heating, mass loss took place due to the decomposition of $CaCO_3$ and $Ca(OH)_2$. It is also possible that a carbothermic reduction reaction may have proceeded even in an N2 atmosphere before the introduction of CO gas. With the introduction of CO reducing gas, mass loss was attributed mainly to the reduction of iron oxides.

The newly studied ettringite-based binder appears to possess several technical, environmental, and economic advantages, including the following:

- Briquettes utilizing ettringite-based binder developed maximum strength after 2 days of curing. This advantage may shorten storage time compared to conventionally produced briquettes.
- The curing of the ettringite-based binder briquettes takes place in ambient conditions. This could potentially save energy and space and reduce costs arising from conventional curing procedures, which involve curing briquettes in high humidity chambers at a temperature of around 30 °C.
- Economic and environmental advantages are achieved when excluding Portland cement from the recipe and replacing it with by-product-based binder.

The reduction program employed in the BFS mimicked conditions at which briquettes may be expected to undergo catastrophic swelling with non-isothermal heating to 950 °C and employing CO as a reducing gas in a BF. Fig. 24 shows contradictory swelling behavior between the reference and LSG briquettes when heated in a nitrogen atmosphere. On the other hand, upon the introduction of CO reducing gas, similar trends in terms of swelling were observed among the briquettes.

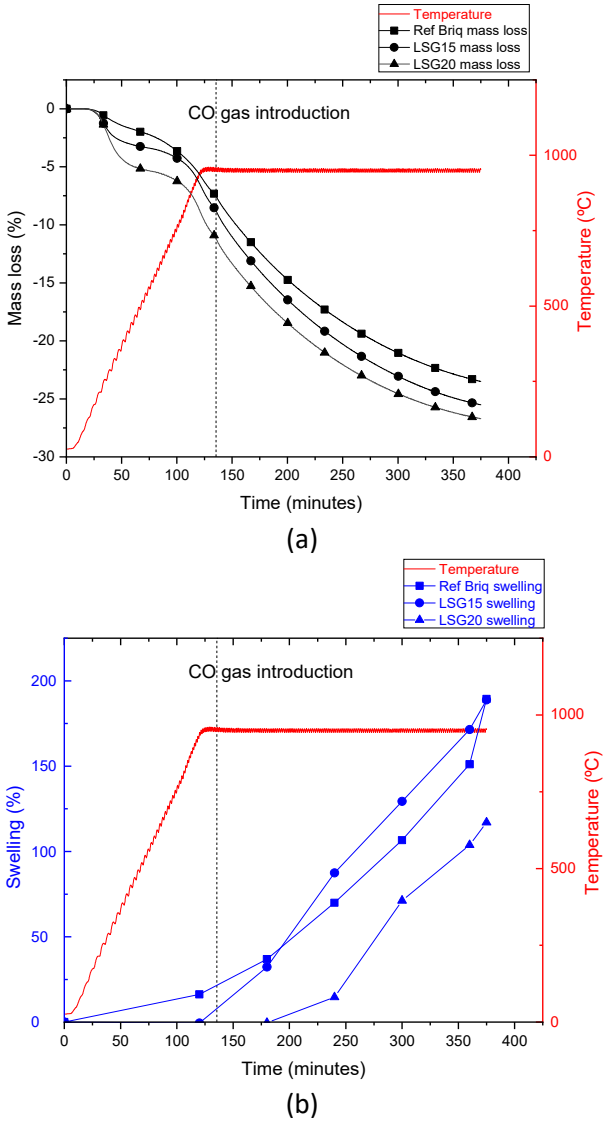

Fig. 24. Reference and LSG briquettes' mass loss (a) and swelling (b) in blast furnace simulator conditions (Reprinted under CC BY 4.0 license from Publication II © 2022 Authors).

5.3 Assessing briquettes' suitability for their use in EAF through laboratory tests

In this research, briquetting trials on a lab scale were carried out to study the suitability of cold-bonded briquettes to be used in an EAF. The briquettes utilized organic and inorganic binders. Organic binders such as dextrose, molasses, and starch were studied as potential replacements for cement in briquette making. Side stream materials and binders were obtained from several industrial partners. Briquetting parameters were optimized. The mechanical properties of the briquettes were evaluated to ensure their adequacy for storage and handling. Drop damage resistance, as well as cold compression tests, were carried out to evaluate the mechanical properties. Advanced thermal tests were carried out to ensure the suitability of the produced briquettes for charging procedures. Such tests included melting trials, optical dilatometer tests, and thermogravimetric analysis coupled with evolved gas analysis using an MS.

The drop damage resistance test results are shown in Fig. 25. Every tested briquette was weighed after each drop. Residual mass (the mass retained by the briquette after being dropped) was recorded. The mass loss of the briquette represents the part of the briquette that disintegrated upon dropping.

In the figure, the residual masses retained by each briquette after every five drops are shown. From the figure, it can be seen that all briquettes except for BRIQ2 and BRIQ5 survived 50 drops without falling below 50% of their original mass. BRIQ1 and BRIQ3 showed similar behavior when tested for drop damage resistance, with briquettes on average falling below 80 and 70% of their original mass, respectively. On the other hand, BRIQ4, BRIQ6, and BRIQ7 achieved high drop damage resistance, surviving all 50 drops and losing less than 5% of their original mass after the test was concluded. BRIQ6 and BRIQ7 lost even less mass compared to the reference ferroalloys (FA) after the test was concluded. BRIQ2's low drop damage resistance may be attributed to the hydration of CaO. As the main constituent of BRIQ2 is conveyor belt fines, lime makes up much of the content of the briquette. Upon the hydration of lime, it transforms into $Ca(OH)_2$, a transformation accompanied by an expansion in volume and leading to higher internal stress within the briquette, lowering its overall strength and deteriorating its mechanical properties. Moreover, porosity appears to play a major role in the resulting mechanical properties of the briquettes. BRIQ2 and BRIQ5 had the highest porosity among the briquettes, at 37.87 and 41.71%, respectively.

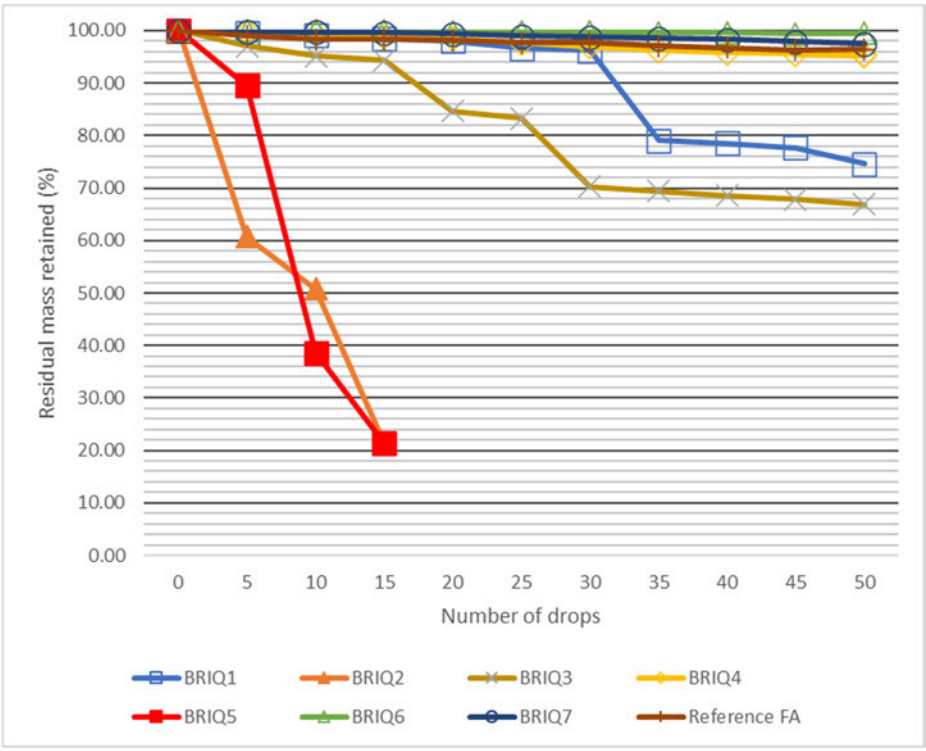

Fig. 25. Drop test results of produced briquettes showing number of drops and residual mass retained after every five drops (Adapted, with permission, from Publication III © 2021 Wiley-VCH GmbH).

The TGA-derivative thermogravimetry (DTG)-MS curves for BRIQ4 are shown in Fig. 26. The combination of DTG and MS curves could accurately indicate which reactions took place during heating. Grinding sludge, oxi-cutting fines, and coal injection are the main components of BRIQ4, with a binder system of starch and paper fibers being used. Grinding sludge contained mainly metallic iron, while magnetite was the main component of the oxi-cutting fines. Other self-reducing briquettes' TGA-DTG-MS test results are discussed elsewhere (Willms et al., 2020).

In Fig. 26, a mass loss of 4.62% when heating the sample to 185 °C can be seen, with a DTG peak occurring at 141.80 °C, indicating moisture evaporation. This is supported by the MS curve, showing a rise in the H_2O signal, which has a mass-to-charge ratio, m/z of 18. The evaporated water originated mainly from the grinding sludge but also from other briquette components. The small peak from the

formation of CO_2 around the same temperature indicates the degradation of the Publication fibers, which made up a small percentage (1.9%) of the briquettes' original mass.

Further heating to 316 °C resulted in a further mass loss of about 7.90%, with a DTG peak formed around 271.80 °C. MS peaks of H_2O (m/z=18), CO (m/z=28), and CO_2 were detected simultaneously, which may be attributed to the degradation of the briquette binder of starch. Starch has been reported to decompose in three stages (Liu et al., 2019). Water evaporates in the first stage upon heating to 120 °C. In the second stage, which takes place around 350 °C, H_2O, CO, CO_2, and CH_4 are released. Finally, in the third stage, which ends at around 600 °C, carbon black is formed. Carbon black may contribute to the reduction of iron oxides at higher temperatures.

During the pyrolysis of coke, carbon monoxide and hydrogen are released, contributing to the reduction of iron oxide in stepwise reactions, according to equations (4)–(6) and (11)–(13). Carbon dioxide and steam evolving from the reduction process then contribute to the gasification of carbon, according to equations (3) and (9). Then, carbon monoxide and hydrogen contribute again to the reduction of iron oxides through the stepwise reduction.

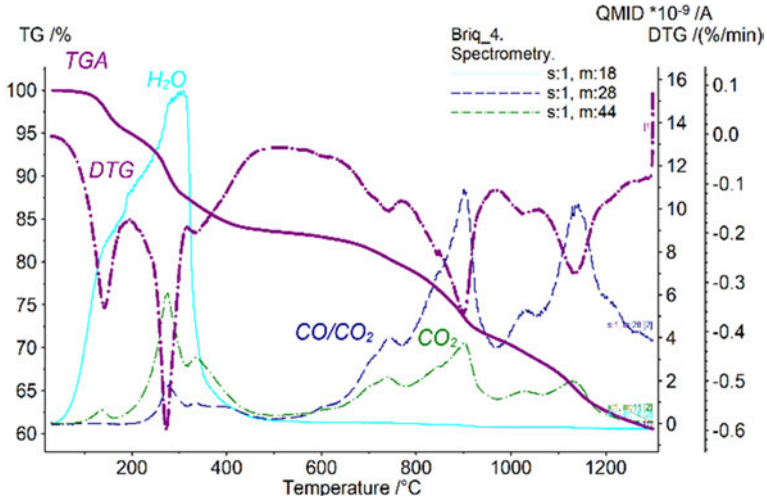

Fig. 26. BRIQ4 TGA-DTG and mass spectrometry at different stages of reduction, showing mass loss and evolving gases (Adapted, with permission, from Publication III © 2021 Wiley-VCH GmbH).

Pieces of approximately 1 cm^3 were cut from BRIQ6 and BRIQ7 to be used in melting trials. BRIQ6 melting behavior was assessed when used with slag from plant 1, while BRIQ7's melting behavior was assessed when used with slag from plant 2. Fig. 27 and Fig. 28 show the different melting stages of BRIQ6 and BRIQ7, respectively. Initially, a flame appeared 15 sec after introducing the briquette sample to the melt. No black smoke or flame was detected after 28 sec, and the sample appeared to start melting. At an interval of 44 sec after introducing the sample, the sample was still detected, with bubbling taking place around the sample. At an interval of 55 sec after introducing the sample, the sample was melted, with only some traces of it visible and more violent bubbling around the remaining traces.

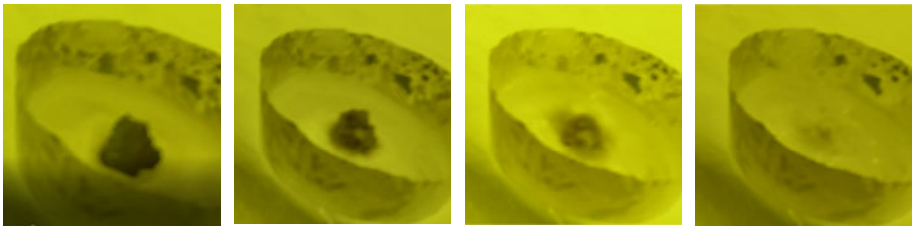

Fig. 27. BRIQ6 briquette directly after placing it on top of plant 1 molten slag (a), after 15 seconds (b), after 25 seconds (c), and after 55 seconds (d) (Adapted, with permission, from Publication III © 2021 Wiley-VCH GmbH).

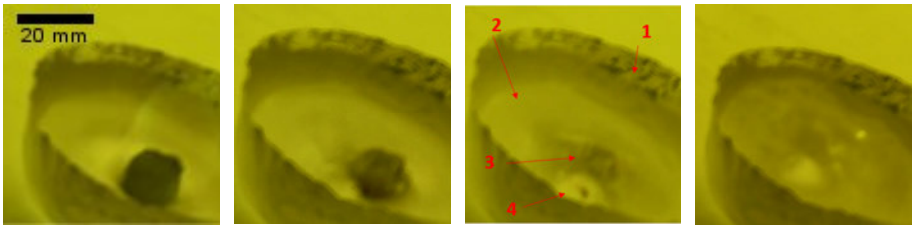

Fig. 28. BRIQ7 briquette directly after placing it on top of plant 2 molten slag (a), after 20 seconds (b), after 30 seconds (c) and after 55 seconds (d). The image shows a platinum crucible (1), molten slag (2), sample remains (3), and bubbling next to the sample (4) (Adapted, with permission, from Publication III © 2021 Wiley-VCH GmbH).

Fig. 29 shows a tested sample from BRIQ3 placed on the sample holder before and after dilatometry testing. The sample used was in a cubic shape of approximately 1 cm^3 and was reduced to a semi sphere metallic drop after the test.

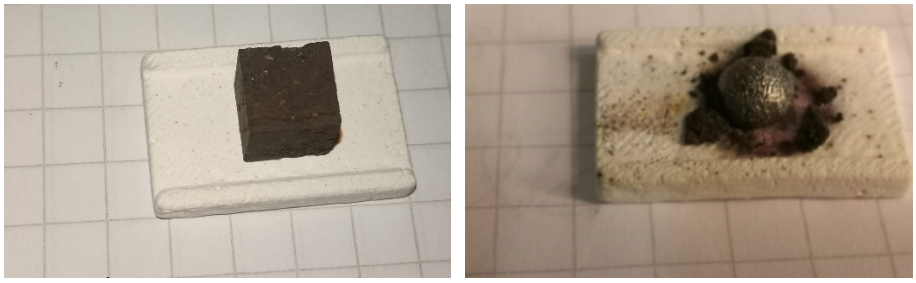

Fig. 29. Dilatometry sample cut in from BRIQ3 placed on a sample holder before (a) and after (b) testing (Adapted, with permission, from Publication III © 2021 Wiley-VCH GmbH).

Fig. 30 shows the BRIQ5 sample at different temperatures during heating in dilatometry testing. BRIQ5 appeared to disintegrate at a low temperature, with disintegration becoming visible at around 180 °C. This indicates that BRIQ5 would be unsuitable for use in an EAF, as it would disintegrate at a low temperature, resulting in the generation of fines.

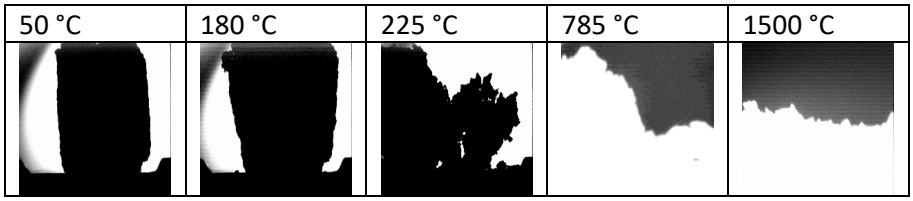

Fig. 30. An example of low temperature disintegration failure of BRIQ5 in dilatometry test (Adapted, with permission, from Publication III © 2021 Wiley-VCH GmbH).

Fig. 31 shows the results of dilatometry testing for BRIQ1, 2, 3, 4, 6, and 7. BRIQ1, 3, and 4 are self-reducing briquettes. They underwent shrinking and then melted into a droplet of iron. On the other hand, slag-forming briquettes, BRIQ2, 6, and 7, only softened at higher temperatures, with BRIQ2 not completely melting up to 1510 °C. BRIQ6 and BRIQ7 melted at temperatures below 1500 °C.

#	Start	Shrinkage	Softening	Melting	End
1	50 °C	1210 °C	1300 °C	1330 °C	1460 °C
	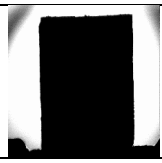		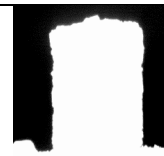	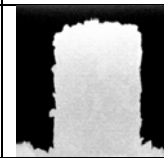	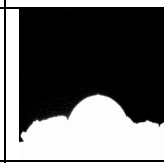
2	50 °C	1420 °C	1450 °C	1495 °C	1510 °C
	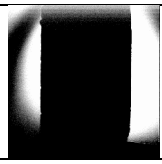	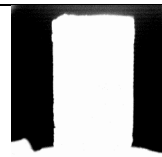	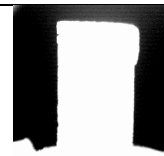	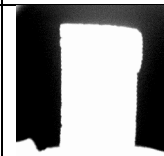	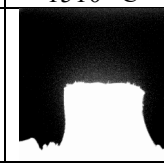
3	50 °C	825 °C	1045 °C	1375 °C	1500 °C
	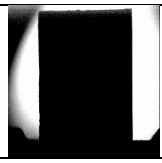	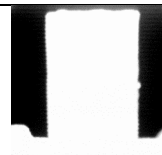	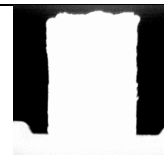	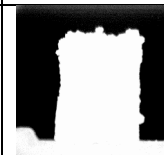	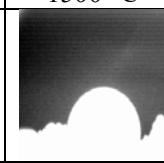
4	50 °C	995 °C	1335 °C	1370 °C	1500 °C
	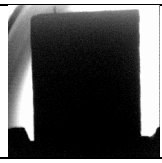	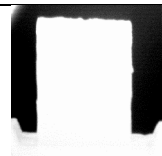	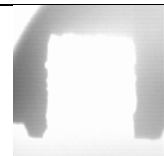	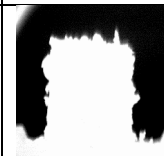	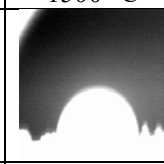
6	50 °C	1380 °C	1385 °C	1395 °C	1500 °C
	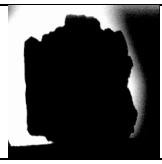	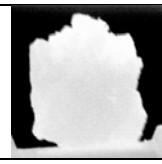	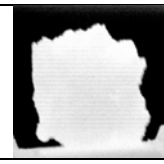	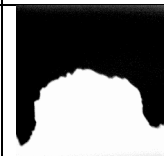	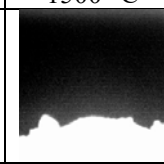
7	50 °C	1340 °C	1380 °C	1395 °C	1465 °C
	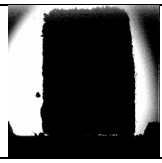	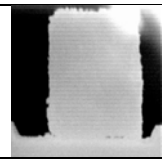	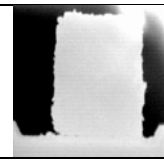	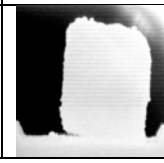	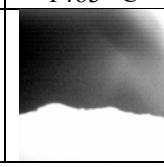

Fig. 31. Results of dilatometry testing for BRIQ1, 2, 3, 4, 6, and 7 (Adapted, with permission, from Publication III © 2021 Wiley-VCH GmbH).

The performance evaluation of briquettes tested for suitability for EAF use is shown in Table 19. BRIQ3 and BRIQ4 were considered suitable to be used in an

EAF. BRIQ1 was considered unsuitable for EAF use, as it generated thick black fumes during reduction tests in BFS. BRIQ2 was also considered unsuitable for EAF use, as it possessed low drop damage resistance. BRIQ5 was also considered unsuitable for EAF use, as it exhibited low temperature disintegration in the dilatometer test and was sensitive to water during sample cutting. Moreover, it had low drop damage resistance. Finally, BRIQ6 and BRIQ7 were considered of limited use, as they were sensitive to water during sample preparation, which might indicate that the storage of briquettes in humid conditions might negatively affect them.

Table 19. Briquette performance evaluation indicated by – for limited, + for suitable, and ++ for excellent performance (Adapted, with permission, from Publication III © 2021 Wiley-VCH GmbH).

Test	Compression	Drop test	TGA- MS	Melting	Reduction	Dilatometry	Sample prep	Suitability
BRIQ1	++	+	+	NA	-	++	+	unsuitable
BRIQ2	+	-	+	NA	NA	+	+	unsuitable
BRIQ3	++	+	+	NA	+	++	+	suitable
BRIQ4	+	++	+	NA	++	++	+	suitable
BRIQ5	+	-	+	NA	+	-	-	unsuitable
BRIQ6	+	++	NA	++	NA	++	-	use limited
BRIQ7	+	++	NA	++	NA	++	-	use limited

6 Conclusion

The target of this thesis was to minimize waste and emissions through hydrogen-assisted reduction of acid iron ore pellets and achieve more sustainable recycling of agglomerates in iron- and steelmaking. This was achieved by the following: (1) studying the influence of H_2 and H_2O on acid pellets' reduction in a CO-CO_2-N_2 atmosphere under simulated BF conditions, (2) developing cold-bonded briquettes using by-product-based ettringite binder from ladle slag, and (3) studying the suitability of self-reducing and slag-forming briquettes for EAF use based on laboratory tests.

The reduction of acid pellets was studied in a temperature range of 700–1100 °C in two different gas mixtures. The reduction of pellets in CO-CO_2-H_2-H_2O-N_2 gas was studied against reduction in CO-CO_2-N_2 gas. The reduction conditions were based on measurements obtained from an operating industrial BF. The presence of hydrogen and the temperature had a positive influence on the degree and rate of reduction. An increased reducing temperature resulted in increased porosity of all tested pellets. The porosity of pellets reduced in CO-CO_2-H_2-H_2O-N_2 gas was higher than that of pellets reduced in CO-CO_2-N_2 gas. On the other hand, an increased temperature resulted in a decrease in BET surface area, except in the range between 900 and 1000 °C. An increase in porosity was accompanied by a decrease in surface decrease, which indicated that fewer but bigger pores were formed with a reduction temperature increase. Pellets reduced in CO-CO_2-H_2-H_2O-N_2 gas had a higher surface area compared with pellets reduced in CO-CO_2-N_2 gas. The higher surface area and higher porosity of pellets reduced in CO-CO_2-H_2-H_2O-N_2 gas contributed to the higher reduction rate and extent of pellets.

Cold-bonded briquettes utilizing ettringite-based binder from ladle slag and gypsum (LSG) were produced at a lab scale. The ettringite-based binder content in briquettes was 10, 15, and 20%. The briquettes' characteristics and performance were compared against a reference briquette produced utilizing ground granulated BF slag and rapid OPC. Side streams used to produce the briquettes were first characterized for their chemical and mineralogical composition, PSD, and physical characteristics. The reference briquette recipe was selected with consideration for optimum particle packing in order to achieve higher strength. LSG briquettes were cured at ambient conditions. Briquettes produced using 10% LSG binder exhibited inferior mechanical properties compared to the reference briquette. Briquettes produced utilizing 15 and 20% LSG binder achieved high early strength and drop damage resistance after 2 and 7 days of curing. The briquettes utilizing 20% LSG

binder achieved higher cold compression strength after 2 days of curing compared to the reference briquette, while briquettes utilizing both 15 and 20% of LSG binder achieved better results than the reference briquette during drop damage resistance tests after 2 and 7 days of curing. Moreover, during reduction tests in a BFS, briquettes utilizing 20% LSG binder exhibited less swelling compared to the reference briquette. LSG binder offers an opportunity to reduce CO_2 emissions in the iron and steel industry, as it utilizes ladle slag, a side stream from the industry, rather than cement. It is also a potentially suitable alternative for ordinary Portland cement in the iron and steel industry because briquette curing could take place in ambient conditions without the need for elevated-temperature humidity chambers. Moreover, briquettes utilizing ettringite-based binder exhibited high early strength development, high drop damage resistance, and less swelling during reduction compared to briquettes utilizing OPC. However, sulfur content originating from gypsum in the binder and the low temperature disintegration due to ettringite dissociation at low temperatures might hinder the use of the briquettes in BFs.

Finally, four self-reducing briquettes and three slag-forming briquettes were assessed through laboratory tests for their suitability to be used in EAFs. Cold compression and drop damage resistance tests were performed to assess the briquettes' mechanical properties and their ability to withstand transportation and handling. TGA-MS and BF simulator tests were performed to assess the heating reduction behavior of the briquettes, and optical dilatometry tests were performed to assess the softening and melting behavior of the briquettes. Melting trials were performed to assess briquettes' interaction with slag melt. Two out of the seven briquettes tested were considered suitable for use in an EAF. Three briquettes were deemed unsuitable for use in an EAF, either due to low temperature disintegration during the dilatometry test, production of high volatiles and thick black fumes during the full briquette testing in a BFS, or low drop damage resistance. Two briquettes were considered to be of limited use, mainly due to their sensitivity to water, which may indicate potential issues during storage in a high-humidity environment.

7 Future work

In this thesis, the influence of H_2-H_2O in CO-CO_2-N_2 gas on the reduction of acid iron ore pellets was studied at temperatures ranging between 700 and 1100 °C. The effect of reducing conditions on iron ore sinters and lump ores should be similarly studied. Moreover, the influence of the charging position of sinter and lump ores could be the subject of future research. Other types of pellets could also be studied to gain an understanding of how the basicity of pellets affects reduction in different atmospheres.

The reduction of pellets, sinter, and iron ore lumps at higher temperatures in different reducing atmospheres could be studied. This could be achieved through TG-MS studies and optical dilatometry studies. Such studies would be helpful in obtaining a better understanding of iron ore softening and melting behavior in conditions simulating those of an operating BF. Moreover, in order to obtain more realistic information regarding iron ore reduction, experiments could be carried out under a load in order to simulate the pressure to which the iron ore is subjected during its descent in the furnace.

Another approach to carrying out the reduction experiments would be to carry out the reduction of different iron ores while in contact with different carbonaceous materials, such as bio coke, coke breeze, and coke dusts. The reduction experiments could take place in pure H_2 gas or pure CO gas to better understand and derive the kinetics parameters. The strength evolution of iron ores during reduction in different atmospheres could also be the subject of a study. This could help to improve the operation of furnaces that involve hydrogen reduction.

In this research, several methods were used to study the suitability of briquettes to be used in EAF. Future extension of the research could focus on creating a systematic and standardized approach to testing the briquettes.

Different cement-free briquettes were studied in this research, several of which showed promising results and appeared adequate to be used in different types of furnaces. An extension of this research could be to study how hydrogen reduction influences briquettes produced using ettringite-based binder or starch. This could help operators to incorporate the studied briquettes in the production process in the future. Future work also could focus on producing binders from side streams that contain lower amounts of sulfur and other harmful elements that may negatively affect the steelmaking process.

References

Adesanya, E., Ohenoja, K., Kinnunen, P., & Illikainen, M. (2017). Properties and durability of alkali-activated ladle slag. *Materials and Structures*, *50*(6), 255. https://doi.org/10.1617/s11527–017–1125–4

Adolfsson, D., Robinson, R., Engström, F., & Björkman, B. (2011). Influence of mineralogy on the hydraulic properties of ladle slag. *Cement and Concrete Research*, *41*(8), 865–871. https://doi.org/10.1016/j.cemconres.2011.04.003

ASTM International. (2018). *ASTM D3038–93, Standard Test Method for Drop Shatter Test for Coke*. ASTM International. https://doi.org/10.1520/D3038–93R18

ASTM International. (2019). *ASTM D440–07, Standard Test Method of Drop Shatter Test for Coal*. ASTM International. https://doi.org/10.1520/D0440–07R19E01

Bagatini, M. C., Zymla, V., Osório, E., & Vilela, A. C. F. (2017). Scale recycling through self-reducing briquettes to use in EAF. *ISIJ International*, *57*(12), 2081–2090. https://doi.org/10.2355/isijinternational.ISIJINT-2017–242

Biswas, A. K. (1981). *Principles of blast furnace ironmaking: Theory and practice*. Cootha.

Blesa, M. J., Miranda, J. L., Izquierdo, M. T., & Moliner, R. (2003). Curing time effect on mechanical strength of smokeless fuel briquettes. *Fuel Processing Technology*, *80*(2), 155–167. https://doi.org/10.1016/S0378–3820(02)00243–6

British Standards Institution. (1986). *Methods for determination of particle size distribution. Part 1: Guide to powder sampling (BS 3406–1:1986)* [Standard]. British Standards Institution (BSI).

British Standards Institution. (1998). *Tests for mechanical and physical properties of aggregates. Part 3: Determination of loose bulk density and voids (BS EN 1097 :1998)* [Standard]. British Standards Institution (BSI).

British Standards Institution. (2007a). *Iron ores for blast furnace and direct reduction feedstocks. Determination of the tumble and abrasion indices. (BS ISO 3271–2007)* [Standard]. British Standards Institution (BSI).

British Standards Institution. (2007b). *Iron ores for blast furnace feedstocks. Determination of the reducibility by the rate of reduction index (BS ISO 4695)* [Standard]. British Standards Institution (BSI).

British Standards Institution. (2015). *Iron ore pellets for blast furnace and direct reduction feedstocks—Determination of the crushing strength (BS ISO 4700:2015)* [Standard]. British Standards Institution (BSI). https://shop.bsigroup.com/ProductDetail/?pid=000000000030132149

Cavaliere, P. (2016). *Ironmaking and steelmaking processes greenhouse emissions, control, and reduction*. Springer.

Chang, J., Zhang, Y., Shang, X., Zhao, J., & Yu, X. (2017). Effects of amorphous AH3 phase on mechanical properties and hydration process of C4A3S ¯-CS¯H2-CH-H2O system. *Construction and Building Materials*, *133*, 314–322. https://doi.org/10.1016/j.conbuildmat.2016.11.111

Choi, S., Kim, J.-M., Han, D., & Kim, J.-H. (2016). Hydration properties of ladle furnace slag powder rapidly cooled by air. *Construction and Building Materials*, *113*, 682–690. https://doi.org/10.1016/j.conbuildmat.2016.03.089

Cypres, R., & Soudan-Moinet, C. (1980). Pyrolysis of coal and iron oxides mixtures. 1. Influence of iron oxides on the pyrolysis of coal. *Fuel*, *59*(1), 48–54. https://doi.org/10.1016/0016–2361(80)90010–1

Darken, L. S., & Gurry, R. W. (1946). The system iron—oxygen. II. Equilibrium and thermodynamics of liquid oxide and other phases. *Journal of the American Chemical Society*, *68*(5), 798–816. https://doi.org/10.1021/ja01209a030

Davydenko, A., Karasev, A., Glaser, B., & Jönsson, P. (2019). Direct reduction of Fe, Ni and Cr from oxides of waste products used in briquettes for slag foaming in EAF. *Materials*, *12*(20), 3434. https://doi.org/10.3390/ma12203434

Davydenko, A., Karasev, A., Lindstrand, G., & Jönsson, P. (2015). Investigation of slag foaming by additions of briquettes in the EAF during stainless steel production. *Steel Research International*, *86*(2), 146–153. https://doi.org/10.1002/srin.201400036

de Araújo, J. A., & Schalch, V. (2014). Recycling of electric arc furnace (EAF) dust for use in steel making process. *Journal of Materials Research and Technology*, *3*(3), 274–279. https://doi.org/10.1016/j.jmrt.2014.06.003

De Belie, N., Soutsos, M., & Gruyaert, E. (Eds.). (2018). *Properties of fresh and hardened concrete containing supplementary cementitious materials: State-of-the-art report of the RILEM technical committee 238-SCM, Working Group 4* (Vol. 25). Springer International Publishing. https://doi.org/10.1007/978–3-319–70606–1

Demus, T., Reichel, T., Schulten, M., Echterhof, T., & Pfeifer, H. (2016). Increasing the sustainability of steel production in the electric arc furnace by substituting fossil coal with biochar agglomerates. *Ironmaking & Steelmaking*, *43*(8), 564–570. https://doi.org/10.1080/03019233.2016.1168564

Dippenaar, R. (2005). Industrial uses of slag (the use and re-use of iron and steelmaking slags). *Ironmaking & Steelmaking*, *32*(1), 35–46. https://doi.org/10.1179/174328105X15805

El-Hussiny, N. A., & Shalabi, M. E. H. (2011). A self-reduced intermediate product from iron and steel plants waste materials using a briquetting process. *Powder Technology*, *205*(1), 217–223.

Gao, J.-T., Li, S.-Q., Zhang, Y.-L., Zhang, Y.-T., & Chen, P.-Y. (2012). Experimental study on solid state recovery of metallic resources from EAF dust. *Ironmaking & Steelmaking*, *39*(6), 446–453. https://doi.org/10.1179/1743281211Y.0000000093

Geerdes, M., Chaigneau, R., Kurunov, I., Lingiardi, O., & Ricketts, J. (2015). *Modern blast furnace ironmaking: An introduction*. IOS Press.

Ghosh, A., & Chatterjee, A. (2010). *Ironmaking and steelmaking: Theory and practice* (3rd printing). PHI Learning.

Godinskii, N. A., Kushnarev, N. N., Yakhshuk, D. S., Kotenev, V. I., & Barsukova, E. Y. (2003). Use of iron-carbon-bearing briquets in electric steelmaking. *Metallurgist*, *47*, 16–19.

Gordon, Y., & Kumar, S. (2013). Selection of ironmaking technology: Principles and risks. *Transactions of the Indian Institute of Metals*, *66*(5–6), 501–513. https://doi.org/10.1007/s12666–013–0267–5

Guézennec, A.-G., Huber, J.-C., Patisson, F., Sessiecq, P., Birat, J.-P., & Ablitzer, D. (2005). Dust formation in electric arc furnace: Birth of the particles. *Powder Technology*, *157*(1–3), 2–11. https://doi.org/10.1016/j.powtec.2005.05.006

Handley, P., & Basuyau, V. (2019). *Legal and environmental bottlenecks and opportunities for slag-based products valorisation*. 15.

Hasanbeigi, A., Arens, M., & Price, L. (2014). Alternative emerging ironmaking technologies for energy-efficiency and carbon dioxide emissions reduction: A technical review. *Renewable and Sustainable Energy Reviews*, *33*, 645–658. https://doi.org/10.1016/j.rser.2014.02.031

Hayes, P. C. (2011). Analysis of product morphologies and reaction mechanisms on gaseous reduction of iron oxides. *Steel Research International*, *82*(5), 480–493. https://doi.org/10.1002/srin.201100032

ISO 7215: 2015. (2015). *Iron ores for blast furnace feedstocks—Determination of the reducibility by the final degree of reduction index*.

Jarnerud, T., Karasev, A. V., & Jönsson, P. G. (2019). Briquetting of wastes from pulp and paper industries by using AOD converter slag as binders for application in metallurgy. *Materials*, *12*(18), 2888. https://doi.org/10.3390/ma12182888

Kemppainen, A., Mattila, O., Heikkinen, E.-P., Paananen, T., & Fabritius, T. (2012). Effect of H2-H2O on the reduction of olivine pellets in CO-CO2 Gas. *ISIJ International*, *52*(11), 1973–1978. https://doi.org/10.2355/isijinternational.52.1973

Kim, J.-M., Choi, S.-M., & Han, D. (2016). Improving the mechanical properties of rapid air cooled ladle furnace slag powder by gypsum. *Construction and Building Materials*, *127*, 93–101. https://doi.org/10.1016/j.conbuildmat.2016.09.102

Kim, S.-H., Zhang, X., Ma, Y., Souza Filho, I. R., Schweinar, K., Angenendt, K., Vogel, D., Stephenson, L. T., El-Zoka, A. A., Mianroodi, J. R., Rohwerder, M., Gault, B., & Raabe, D. (2021). Influence of microstructure and atomic-scale chemistry on the direct reduction of iron ore with hydrogen at 700 °C. *Acta Materialia*, *212*, 116933. https://doi.org/10.1016/j.actamat.2021.116933

Koros, P. J. (2003). Dusts, scale, slags, sludges... Not wastes, but sources of profits. *Metallurgical and Materials Transactions B*, *34*(6), 769–779.

Kumar, D. S., Sah, R., Sekhar, V. R., & Vishwanath, S. C. (2017). Development and use of mill scale briquettes in BOF. *Ironmaking & Steelmaking*, *44*(2), 134–139. https://doi.org/10.1080/03019233.2016.1165499

Lecacheux, B., Bailly, J. L., Sert, D., Bolsigner, J. P., Iezzi, J., Maurice, Y., Lusson, F., Degrave, S., Daelman, A., & Vanhaelst, K. (2011). *Characterization of blast furnace operation by means of multi-points vertical probing technology*. 8.

Liu, Y., Yang, L., Ma, C., & Zhang, Y. (2019). Thermal behavior of sweet potato starch by non-isothermal thermogravimetric cAnalysis. *Materials*, *12*(5), 699. https://doi.org/10.3390/ma12050699

López, F. A., & López-Delgado, A. (2002). Enhancement of electric arc furnace dust by recycling to electric arc furnace. *Journal of Environmental Engineering*, *128*(12), 1169–1174. https://doi.org/10.1061/(ASCE)0733–9372(2002)128:12(1169)

Luz, C. A., Pera, J., Cheriaf, M., & Rocha, J. C. (2007). Behaviour of calcium sulfoaluminate cement in presence of high concentrations of chromium salts. *Cement and Concrete Research*, *37*(4), 624–629. https://doi.org/10.1016/j.cemconres.2006.11.018

Magdziarz, A., Ku, M., & Hryniewicz, M. (2015). Briquetting of EAF dust for its utilisation in metallurgical processes. *Chemical and Process Engineering*, 9.

Mahasenan, N., Smith, S., & Humphreys, K. (2003). The cement industry and global climate change: current and potential future cement industry CO2 emissions. In *Greenhouse Gas Control Technologies—6th International Conference: Vol. II* (pp. 995–1000). Elsevier. https://doi.org/10.1016/B978–008044276–1/50157–4

Manso, J. M., Losañez, M., Polanco, J. A., & Gonzalez, J. J. (2005). Ladle furnace slag in construction. *Journal of Materials in Civil Engineering*, *17*(5), 513–518. https://doi.org/10.1061/(ASCE)0899–1561(2005)17:5(513)

Matthew, S. P., & Hayes, P. C. (1990). Microstructural changes occurring during the gaseous reduction of magnetite. *Metallurgical Transactions B*, *21*(1), 153–172. https://doi.org/10.1007/BF02658127

Ministry of Economic Affairs and Employment, Ministry of the Environment, Ministry of Agriculture and Forestry, Ministry of Transport and Communications, & Ministry of Finance. (2019). *Finland's integrated energy and climate plan*. Ministry of Economic Affairs and Employment. http://julkaisut.valtioneuvosto.fi/bitstream/handle/10024/161977/TEM_2019_66.pdf?sequence=1&isAllowed=y

Moukassi, M., Steinmetz, P., Dupre, B., & Gleitzer, C. (1983). A study of the mechanism of reduction with hydrogen of pure wustite single crystals. *Metallurgical Transactions B*, *14B*, 125–132.

Mousa, E. A., Ahmed, H. M., & Wang, C. (2017). Novel approach towards biomass lignin utilization in ironmaking blast Furnace. *ISIJ International*, *57*(10), 1788–1796. https://doi.org/10.2355/isijinternational.ISIJINT-2017–127

Ndlovu, S., Simate, G. S., & Matinde, E. (2017). *Waste production and utilization in the metal extraction industry* (1st ed.). CRC Press, Taylor & Francis Group. https://doi.org/10.1201/9781315153896

Nguyen, H., Adesanya, E., Ohenoja, K., Kriskova, L., Pontikes, Y., Kinnunen, P., & Illikainen, M. (2019). Byproduct-based ettringite binder – A synergy between ladle slag and gypsum. *Construction and Building Materials*, *197*, 143–151. https://doi.org/10.1016/j.conbuildmat.2018.11.165

Omran, M., Fabritius, T., & Abdelrahim, A. (2020). Effect of metallurgical waste properties on determining suitable recycling method. *Key Engineering Materials*, *835*, 297–305. https://doi.org/10.4028/www.scientific.net/KEM.835.297

Paknahad, P., Askari, M., & Shahahmadi, S. A. (2019). Cold-briquetted iron and carbon (CBIC): Investigation of the influence of environmental condition on its chemical and physical properties. *Journal of Sustainable Metallurgy*, *5*(4), 497–509. https://doi.org/10.1007/s40831–019–00240-y

Papayianni, I., & Anastasiou, E. (2012). Effect of granulometry on cementitious properties of ladle furnace slag. *Cement and Concrete Composites*, *34*(3), 400–407. https://doi.org/10.1016/j.cemconcomp.2011.11.015

Peysson, S., Péra, J., & Chabannet, M. (2005). Immobilization of heavy metals by calcium sulfoaluminate cement. *Cement and Concrete Research*, *35*(12), 2261–2270. https://doi.org/10.1016/j.cemconres.2005.03.015

Pineau, A., Kanari, N., & Gaballah, I. (2006). Kinetics of reduction of iron oxides by H2: Part I: Low temperature reduction of hematite. *Thermochimica Acta*, *447*(1), 89–100. https://doi.org/10.1016/j.tca.2005.10.004

Pineau, A., Kanari, N., & Gaballah, I. (2007). Kinetics of reduction of iron oxides by H2: Part II. Low temperature reduction of magnetite. *Thermochimica Acta*, *456*(2), 75–88. https://doi.org/10.1016/j.tca.2007.01.014

Posch, W., Presslinger, H., & Hiebler, H. (2002). Mineralogical evaluation of ladle slags at voestalpine Stahl GmbH. *Ironmaking & Steelmaking*, *29*(4), 308–312. https://doi.org/10.1179/030192302225005169

Proctor, D. M., Fehling, K. A., Shay, E. C., Wittenborn, J. L., Green, J. J., Avent, C., Bigham, R. D., Connolly, M., Lee, B., Shepker, T. O., & Zak, M. A. (2000). Physical and chemical characteristics of blast furnace, basic oxygen furnace, and electric arc furnace steel industry slags. *Environmental Science & Technology*, *34*(8), 1576–1582. https://doi.org/10.1021/es9906002

Qie, Y., Lyu, Q., Li, J., Lan, C., & Liu, X. (2017). Effect of hydrogen addition on reduction kinetics of iron oxides in gas-injection BF. *ISIJ International*, *57*(3), 404–412. https://doi.org/10.2355/isijinternational.ISIJINT-2016–356

Raabe, D., Tasan, C. C., & Olivetti, E. A. (2019). Strategies for improving the sustainability of structural metals. *Nature*, *575*(7781), 64–74. https://doi.org/10.1038/s41586–019–1702–5

Rađenović, A., Malina, J., & Sofilić, T. (2013). Characterization of ladle furnace slag from carbon steel production as a potential adsorbent. *Advances in Materials Science and Engineering*, *2013*, 1–6. https://doi.org/10.1155/2013/198240

Rao, S. R. (2006). *Resource recovery and recycling from metallurgical wastes* (Vol. 7). Elsevier. https://doi.org/10.1016/S0713–2743(06)X8083–2

Ray, H. S., & Ray, S. (2018). *Kinetics of metallurgical processes*. Springer. http://dx.doi.org/10.1007/978–981–13–0686–0

Richards, S. R. (1990). Physical testing of fuel briquettes. *Fuel Processing Technology*, *25*(2), 89–100.

Seetharaman, S. (2005). *Fundamentals of metallurgy*. Woodhead Pub. and Maney Pub. on behalf of the Institute of Materials, Minerals and Mining ; CRC Press.

Seetharaman, S., McLean, A., Guthrie, R., & Seshadri, S. (Eds.). (2014). *Treaties on Process Metallurgy Industrial Processes, Part A*. Elsevier.

Setién, J., Hernández, D., & González, J. J. (2009). Characterization of ladle furnace basic slag for use as a construction material. *Construction and Building Materials*, *23*(5), 1788–1794. https://doi.org/10.1016/j.conbuildmat.2008.10.003

Shi, C. (2002). Characteristics and cementitious properties of ladle slag fines from steel production. *Cement and Concrete Research*, *32*(3), 459–462. https://doi.org/10.1016/S0008–8846(01)00707–4

Shi, C., & Hu, S. (2003). Cementitious properties of ladle slag fines under autoclave curing conditions. *Cement and Concrete Research*, *33*(11), 1851–1856. https://doi.org/10.1016/S0008–8846(03)00211–4

Singh, M., & Bjorkman, B. (2006). Strength of cement-bonded briquettes. *Minerals and Metallurgical Processing*, *23*(4), 203–213.

Spreitzer, D., & Schenk, J. (2019). Reduction of iron oxides with hydrogen—A review. *Steel Research International*, 1900108. https://doi.org/10.1002/srin.201900108

Suetens, T., Van Acker, K., Blanpain, B., Mishra, B., & Apelian, D. (2014). Moving towards better recycling options for electric arc furnace dust. *The Minerals, Metals & Materials Society*, *66*(7), 1119–1121. https://doi.org/10.1007/s11837–014–1044–6

Sundqvist Ökvist, L., Jonsson, K., Lampinen, H., & Eriksson, L. (1999). *Recycling of in-plant fines as cold-bonded agglomerates*. https://www.lkab.com/en/SysSiteAssets/dokument/kund/1999-recycling-of-in-plant-fines-as-cold-bonded--agglomerates.pdf

Taylor, H. F. W. (1997). *Cement chemistry* (2nd ed.). T. Telford.

Toulouevski, Y. N., & Zinurov, I. Y. (2013). *Innovation in electric arc furnaces*. Springer. https://doi.org/10.1007/978–3-642–36273–6

Turkdogan, E. T. (2010). *Fundamentals of steelmaking*. Institute of Materials. http://site.ebrary.com/id/10421371

Wagner, D., Devisme, O., Patisson, F., & Ablitzer, D. (2006). *A laboratory study of the reduction of iron oxides by hydrogen*. *2*, 111–120.

Willms, T., Echterhof, T., Steinlechner, S., Aula, M., Abdelrahim, A., Fabritius, T., Mombelli, D., Mapelli, C., & Preiss, S. (2020). Investigation on the chemical and thermal behavior of recycling agglomerates from EAF by-products. *Applied Sciences*, *10*(22), 8309. https://doi.org/10.3390/app10228309

Winnefeld, F., & Lothenbach, B. (2010). Hydration of calcium sulfoaluminate cements—Experimental findings and thermodynamic modelling. *Cement and Concrete Research*, *40*(8), 1239–1247. https://doi.org/10.1016/j.cemconres.2009.08.014

Worldsteel Association. (2022). *World Steel in Figures 2022*.

Yang, Q., Holmberg, N., & Björkman, B. (2009). EAF smelting trials of waste-carbon briquettes at Avesta Works of Outokumpu Stainless AB for recycling oily mill scale sludge from stainless steel production. *Steel Research International*, *80*(6), 422–428. https://doi.org/10.2374/SRI09SP003

Yilmaz, C., Wendelstorf, J., & Turek, T. (2017). Modeling and simulation of hydrogen injection into a blast furnace to reduce carbon dioxide emissions. *Journal of Cleaner Production*, *154*, 488–501. https://doi.org/10.1016/j.jclepro.2017.03.162

Original publications

I Abdelrahim, A., Iljana, M., Omran, M., Vuolio, T., Bartusch, H., & Fabritius, T. (2020). Influence of H_2–H_2O content on the reduction of acid iron ore pellets in a CO–CO_2–N_2 reducing atmosphere. ISIJ International, 60, 2206. https://doi.org/10.2355/isijinternational.ISIJINT-2019–734

II Abdelrahim, A., Nguyen, H., Omran, M., Kinnunen, P., Iljana, M., Illikainen, M., & Fabritius, T. (2022). Development of Cold-Bonded Briquettes Using By-Product-Based Ettringite Binder from Ladle Slag. Journal of Sustainable Metallurgy, 8(1), 468–487. https://doi.org/10.1007/s40831–022–00511–1

III Abdelrahim, A., Aula, M., Iljana, M., Willms, T., Echterhof, T., Steinlechner, S., Mombelli, D., Mapelli, C., Omran, M., Preiss, S., & Fabritius, T. (2021). Suitability of Self-Reducing and Slag-Forming Briquettes for Electric Arc Furnace Use Based on Laboratory Tests. Steel Research International, 2100472. https://doi.org/10.1002/srin.202100472

Original publications are not included in the electronic version of the dissertation.

[1] https://creativecommons.org/licenses/by/4.0/

Book orders:
Virtual book store
https://verkkokauppa.omapumu.com/fi/

UNIVERSITY OF OULU P.O. Box 8000 FI-90014 UNIVERSITY OF OULU FINLAND

ACTA UNIVERSITATIS OULUENSIS

ISBN 978-952-62-3652-0 (Paperback)
ISBN 978-952-62-3653-7 (PDF)
ISSN 0355-3213 (Print)
ISSN 1796-2226 (Online)

UNIVERSITY OF OULU